(2) LEVEL

AD A066039

DDC FILE COPY

# EXPERIMENTAL SERIES PARAMETERS FOR THE DECAY OF MULTIGROUP BETA AND GAMMA SPECTRA FROM 0.1 TO 1000 SECONDS AFTER A FISSION BURST
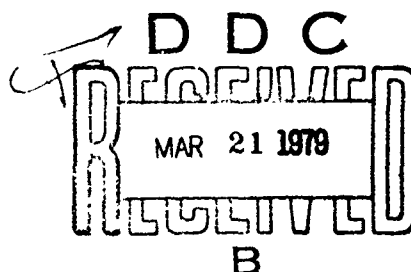
D. Graham Foster, Jr., T. R. England, and N. L. Whittemore

Los Alamos Scientific Laboratory
P.O. Box 1663
Los Alamos, New Mexico 87545

November 1978

Final Report

D D C
RECEIVED
MAR 21 1979
B

79 03 07 023

This final report was prepared by the Los Alamos Scientific Laboratory, Los Alamos, New Mexico, under Project Order 77-096, Job Order 88091901 with the Air Force Weapons Laboratory, Kirtland Air Force Base, New Mexico. Lt William G. Kuller (DYCE) was the Laboratory Project Officer-in-Charge.

When US Government drawings, specifications, or other data are used for any purpose other than a definitely related Government procurement operation, the Government thereby incurs no responsibility nor any obligation whatsoever, and the fact that the Government may have formulated, furnished, or in any way supplied the said drawings, specifications, or other data, is not to be regarded by implication or otherwise, as in any manner licensing the holder or any other person or corporation, or conveying any rights or permission to manufacture, use, or sell any patented invention that may in any way be related thereto.

This report has been reviewed by the Office of Information (OI) and is releasable to the National Technical Information Service (NTIS). At NTIS, it will be available to the general public, including foreign nations.

This report has been authored by a contractor of the United States Government. Accordingly, the United States Government retains a nonexclusive, royalty-free license to publish or reproduce the material contained herein, or allow others to do so, for the United States Government purposes.

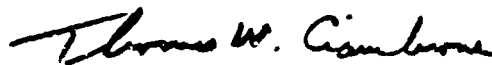This technical report has been reviewed and is approved for publication.


WILLIAM G. KULLER
1LT, USAF
Project Officer


FOR THE COMMANDER


JOHN D. HAWKINS
Major, USAF
Chief, Satellite and $C^3$ Branch

THOMAS W. CIAMBRONE
Lt Colonel, USAF
Chief, Applied Physics Division

# REPORT DOCUMENTATION PAGE

READ INSTRUCTIONS
BEFORE COMPLETING FORM

| 1. REPORT NUMBER | 2. GOVT ACCESSION NO. | 3. RECIPIENT'S CATALOG NUMBER |
|---|---|---|
| AFWL-TR-78-4 | | |

**4. TITLE (and Subtitle)**

EXPERIMENTAL-SERIES PARAMETERS FOR THE DECAY OF MULTIGROUP BETA AND GAMMA SPECTRA FROM 0.1 TO 1000 SECONDS AFTER A FISSION BURST.

**5. TYPE OF REPORT & PERIOD COVERED**

Final Report

**6. PERFORMING ORG. REPORT NUMBER**

**7. AUTHOR(s)**

D. Graham Foster, Jr., T. R. England,
N. L. Whittemore

**8. CONTRACT OR GRANT NUMBER(s)**

**9. PERFORMING ORGANIZATION NAME AND ADDRESS**

Los Alamos Scientific Laboratory
P.O. Box 1663
Los Alamos, New Mexico 87545

**10. PROGRAM ELEMENT, PROJECT, TASK AREA & WORK UNIT NUMBERS**

626210
88091 901

**11. CONTROLLING OFFICE NAME AND ADDRESS**

Air Force Weapons Laboratory (DYCE)
Kirtland AFB, New Mexico 87117

**12. REPORT DATE**

November 1978

**13. NUMBER OF PAGES**

62

**14. MONITORING AGENCY NAME & ADDRESS(If different from Controlling Office)**

SPIL

**15. SECURITY CLASS. (of this report)**

UNCLASSIFIED

**15a. DECLASSIFICATION/DOWNGRADING SCHEDULE**

**16. DISTRIBUTION STATEMENT (of this Report)**

Approved for public release; distribution unlimited

AD-£ʒ00 240

**17. DISTRIBUTION STATEMENT (of the abstract entered in Block 20, if different from Report)**

**18. SUPPLEMENTARY NOTES**

This research was funded by AFSC/DL; Project Order No. 77-096

**19. KEY WORDS (Continue on reverse side if necessary and identify by block number)**

| | |
|---|---|
| Fission Product Decay | Magnetosphere |
| Beta Spectrum | Nuclear Explosion |
| Gamma Spectrum | Least Squares Fit |

**20. ABSTRACT (Continue on reverse side if necessary and identify by block number)**

Accurate predictions of beta and gamma spectra as a function of time following neutron-induced fission can be made by summation calculations from the fission-product data in the Evaluated Nuclear Data File, Part B(ENDF/B), but the calculations are expensive and the data base is very large. A multigroup spectrum can be represented sufficiently accurately over a limited time range by a few-term exponential series obtained by least-squares fitting to the summation calculations. This report summarizes the preparation of such a parameter set for the

(over)

DD FORM 1473 EDITION OF 1 NOV 65 IS OBSOLETE

013 150 79 03 07 02

20. ABSTRACT (Cont'd)

Air Force Weapons Laboratory (AFWL). The set describes decay of beta and gamma spectra from 0.1 to 1000 seconds after fission of $^{235}U$, $^{238}U$, or $^{239}Pu$ induced by fission-spectrum or 14-MeV neutrons. Fits that are as accurate as the ENDF/B data warrant can be made with five or fewer terms per energy group. An alternative set of parameters that uses the same decay constants in each group for all six combinations of isotope and neutron energy, but different amplitudes for each combination, requires only one additional term for comparable accuracy.

# SUMMARY

Many applied problems would benefit from being able to describe postfission decay of beta or gamma spectra accurately over a limited range of times by only a small number of parameters. This report describes the preparation of such a set by least-squares fitting of a series of exponential functions to each group in selected multigroup spectra calculated by summation of fission-product data in ENDF/B. The parameters are for fission of $^{235}U$, $^{238}U$, and $^{239}Pu$ induced by fission-spectrum and 14-MeV neutrons. They cover the time range from 0.1 to 1000 seconds after fission.

Approximately 45% of the photons emitted from zero to infinite decay time emerge in the first millisecond after fission. These are not included in the data set described in this report. Of all beta particles emitted from the instant of fission, or all gamma rays emitted after the first millisecond, about 70% emerge during the 0.1-to-1000-second interval covered by our fits. Extrapolation of our fits to infinite time misses an average of about 5% of the postmillisecond yield.

The ENDF/B data have uncertainties in total energy-release rates of less than 10% for decay times greater than about 100 seconds. The fits can achieve few-percent accuracy with five or fewer terms in the series. At the expense of one additional term, a given fitting accuracy can be achieved with a more compact parameter set that uses a single set of decay constants per group for all six combinations of fissioning isotope and neutron energy but individual amplitudes for each combination. We find the earlier work by Dieckhoner on the beta spectrum from $^{235}U$ irradiated by fission-spectrum neutrons to be in moderately good agreement with modern data near the peak in the spectrum for several decay times, but in poor agreement elsewhere. We anticipate a substantial improvement in reliability of calculations like ours when Version 5 of ENDF/B is released, particularly for the short decay times emphasized in this work.

1

## PREFACE

The work described in this report would have been impossible without the preexisting code system and data base developed with the support of several agencies of the U.S. Government. The fission-product data in ENDF/B are the fruit of a long-term program of the Division of Reactor Development and Demonstration of the U.S. Energy Research and Development Agency (ERDA) (now Department of Energy). The U.S. Nuclear Regulatory Commission supported the evolution of the computer program CINDER-7 into CINDER-10, the development of the programs FPDCYS and FPSPEC, and the use of CINDER-10 in processing five of the six basic data sets used in the present work. AFWL, to whom this report is addressed, supported the reduction of preliminary Version-5 ENDF/B data to individual-nuclide fission yields for 14-MeV neutrons on $^{239}$Pu and the corresponding processing through CINDER. AFWL also supported processing of all of the data through a streamlined version of FPSPEC, as well as the development and use of the program FPSPFT and its ancillary codes (which constituted the main part of the present work). ERDA's Division of Military Applications furnished supporting services in the preparation of this report.

CONTENTS

## ILLUSTRATIONS

(ILLUSTRATIONS, continued)

## TABLES

## SECTION I

## INTRODUCTION

This report describes the preparation, for the Air Force Weapons Laboratory (AFWL), of a compact parameterization of the beta and gamma spectra emitted by fission products during the interval from 0.1 to 1000 seconds after a very short fission burst. Although this project was designed specifically to supply input to computer codes that calculate the injection of electrons from a high-altitude nuclear explosion into the earth's magnetosphere, the results have obvious applications to other problems. Indeed, the gamma spectra were included without any immediate objective in mind, taking advantage of the fact that they constituted an inexpensive add-on to the beta spectra. The parameterization that we have used is least-squares fitting of a series of exponential functions.

The specific task for which this work was performed has had the effect of limiting its scope in two respects. In the first place, since it is intended to be applied to nuclear explosions, the resulting parameter set is restricted to fission of $^{235}$U, $^{238}$U, and $^{239}$Pu by fission neutrons and by 14-MeV neutrons. Although data are available for thermal neutrons, these have not been included in the set because practical nuclear explosives make negligible use of thermal neutrons. In the second place, the time range of 0.1 to 1000 seconds after fission excludes interesting phenomena at both earlier and later times. Both limits were chosen to permit a quick, accurate solution with a minimum number of parameters. Thus, although the electron spectrum should extrapolate accurately to zero time, the parameterized photon spectrum does not include the intense prompt burst or succeeding decay of metastable states of the primary fission products prior to one millisecond, which constitute the source of the electromagnetic pulse that follows a nuclear explosion. Both electron and photon yield curves exhibit a pronounced kink between $10^3$ and $10^4$ seconds after fission. Fitting these would have required several additional parameters in order to describe fewer than 15% of the electrons injected into the magnetosphere, and would have increased the cost and duration of this project in exchange for minimal practical gain.

Our basic approach is usually described as a summation calculation. It continues the trend exemplified by the earlier work of Stovall (ref. 1)

and of Dieckhoner (ref. 2). Rather than work from direct measurements of time-dependent spectra, of which there are not nearly enough to cover the requirements of this project, we have reconstructed the spectra from detailed data on each step in the fission-and-decay process. This was possible within the existing budgetary constraints only because other sponsors* had already supported most of the data preparation, and the prepared data were stored in the Central Computing Facility of the Los Alamos Scientific Laboratory (LASL) in machine-readable form. The only basic data added specifically for this project were fission yields for 14-MeV neutrons irradiating $^{239}$Pu.

Section II of this report describes this data base in greater detail, and summarizes the initial computational procedure, including the parts that had already been completed before this project began. Section III gives a general overview of the resulting time-dependent spectra. Section IV discusses the extensive program of validating the data and the computational procedures by comparison to benchmark experiments. Section V gives an explicit comparison of the present results with those of Dieckhoner (ref. 2). Section VI describes the form and procedure for parameterizing the time-dependent spectra for use by AFWL. Section VII discusses extensions and improvements to both the data and the fitting process that could profitably be exploited in the future. As an aid to actual use of the AFWL parameter set, we have included appendices that describe the mathematics of the fit and the format of both the output listings from the fitting program and the cards used for transmitting the fitted parameters.

Since we shall refer frequently to energy-isotope cases; that is, to specific combinations of neutron energy and fissioning nuclide, we shall henceforth use the abbreviations for these cases listed in table 1. The last column of the table lists the number of individual decay times for which we have spectra available for fitting in the time range between 0.1 and 1000 seconds after fission.

---

*See the preface to this report for the contributions supported by each sponsor.

Table 1

ABBREVIATIONS USED TO DESIGNATE DATA SETS

| Fissioning Nuclide | Neutron Energy | Abbreviation | Number of Decay Times, 0.1-1000 s |
|---|---|---|---|
| $^{235}U$ | thermal | 25T | 29 |
| $^{239}Pu$ | thermal | 49T | 29 |
| $^{235}U$ | fiss. spec.* | 25F | 9 |
| $^{238}U$ | fiss. spec.* | 28F | 29 |
| $^{239}Pu$ | fiss. spec.* | 49F | 29 |
| $^{235}U$ | 14 MeV | 25H | 9 |
| $^{238}U$ | 14 MeV | 28H | 9 |
| $^{239}Pu$ | 14 MeV | 49H | 29 |

*Fiss. spec. = fission-spectrum neutrons

## SECTION II

## CALCULATION OF TIME-DEPENDENT SPECTRA

All of the data used in this work are taken from the Evaluated Nuclear
Data File, part B (ref. 3), which is customarily abbreviated ENDF/B. The
individual-nuclide yields of the fission products from 14-MeV fission of $^{239}$Pu
(case 49H) are taken from a preliminary set for Version 5 of ENDF/B; all other
data are from Version 4. Table 2 summarizes the nature and extent of the data
in ENDF/B-4. Most of the data are from actual measurements, but some of the
half-lives and decay energies have been taken from nuclear systematics, espe-
cially for nuclides with half-lives less than one second. In Version 5 im-
proved models have been used to supplement measurements in distributing the
mass-chain yields among the individual nuclides in each chain. In particular,
Madland and England (ref. 4), find that a correction for the effect of the
nuclear pairing force varies greatly from one fissioning nuclide to another
for low neutron energies, but has only a minor effect at 14 MeV. In ref. 5
the same authors describe a semiempirical model for the ratio of yields to
the ground and isomeric states of the same nucleus. In the past it has been
assumed, in the absence of measurements, that the two states are populated
equally, whereas Madland and England find that the isomeric state is usually
strongly favored.

### Table 2

### SUMMARY OF ENDF/B-4 FISSION-PRODUCT DATA

825 nuclides (total, counting isomers separately)

112 isomers with half lives > 0.1 second

 42 different elements

 96 different mass numbers

 77 nuclides marked as gaseous isotopes of 4 elements

181 have neutron-interaction cross sections

180 have explicit data on beta and/or gamma spectra

712 are unstable and have average $\alpha$, $\beta$, and $\gamma$ energy
and branching fraction

825 have fission yields for each of 6 fissionable
nuclides ($\sim 10^4$ yields) for one or more ranges
of neutron energy

ENDF/B data were originally strongly oriented towards the needs of the reactor-design community. Accordingly, experimental data and theoretical interpolations now in the files emphasize energy production rather than particle spectra. The spectral data are concentrated on times greater than a minute after fission and on fission induced by thermal neutrons. Thus, the data do not serve our particular needs as well as they do the needs of reactor design.

The primary code that LASL uses (ref. 6) for generating the time dependence of fission-product decay is CINDER (currently CINDER-10). Although it was developed earlier and entirely independently, CINDER contains substantially all of the features recommended by Dieckhoner (ref. 2), in addition to having access to the vast amount of recent data in ENDF/B. It calculates production and depletion of fission products by applying a known neutron-flux history to multigroup cross sections taken from ENDF/B. In the present application to essentially instantaneous fission we have uniformly used a constant flux of $10^{13}/(s \cdot cm^2)$ applied for $10^{-4}$ seconds. Decay is followed along the mass chains, as well as between chains when delayed neutrons are emitted. The actual coupled decay scheme of 825 nuclides is decomposed into linearized chains containing 2811 nuclides, of which 1722 are out-of-sum virtual members to eliminate double counting of partial yields and the rest are summed to give the actual yields. CINDER solves the linearized chains using a completely general solution to the coupled differential equations. Because some of the chains contain as many as twenty members, very careful attention has been given to preventing the accumulation of rounding errors. CINDER output lists the concentration, activity, and energy-emission rate for each nuclide (including isomers) separately as well as their overall sums. In addition, gaseous and volatile-solid isotopes are summed separately.

The 180 nuclides that have detailed spectra in ENDF/B have been processed separately by the code FPDCYS (ref. 7). FPDCYS uses the exact Fermi expressions to generate beta spectra from the tabulated end-point energies, transition types, and branching ratios, then calculates the integrals over 75 100-keV bins. The tabulated gamma-ray line spectra from ENDF/B are simply binned into 125 50-keV groups. Both sets of spectra are stored for use by other codes. For our project we have sorted the spectra into a standard order and placed them in a compact binary library for rapid retrieval. Similarly, we have picked up from the stored output of CINDER the individual-nuclide data as a

function of decay time, sorted them into the same standard sequence, and stored them in another binary library along with the parameters that describe the irradiation history.

The final step in generating the composite spectra is to combine the stored spectra from FPDCYS with the stored irradiation parameters and time-dependent decay-rates from CINDER, using a code named FPSPEC (ref. 7). The result is absolute particle-emission rates per fission from the 180 nuclides with known spectra (ref. 8). The CINDER calculations also supply the total electron and photon energy-emission rates for these nuclides, and independently for the entire ensemble of 825 fission products. Since we have no further information available, we assume that the average spectrum of the remaining 645 nuclides is the same as that of the 180, and normalize the calculated spectrum to the total beta or gamma energy-emission rate. We shall consider the validity of this normalization in Sections III and IV. FPSPEC stores these normalized spectra in a cumulative binary library of its own, to serve as input to the exponential-fitting process.

The CINDER output used in this project was generated at various times during 1976 and 1977 for various immediate purposes. The earliest data sets contained calculations only at decay times of 1 and 5 times powers of 10 seconds. Using the notation of table 1, sets 25F, 25H, and 28H are of this type. These "sparse" sets have only nine times in the range 0.1 to $10^3$ seconds, which seriously restricts the fitting operation. More recently, sets 28H and 49F were rerun to add points at 1.5, 2, 4, 6, and 8 in each time decade, raising the total to 29 times per set. We shall call these "dense" sets. The only case run expressly for this project, 49H, is also dense, but in each decade we have substituted a point at 3 for the one at 5 to produce a more even logarithmic spacing. The number of decay times per case is included in table 1.

12

SECTION III

GENERAL OVERVIEW OF TIME-DEPENDENT SPECTRA

Our normalization method insures that the total energy-emission rate
implied by our calculated spectra will be as accurate as any quantity that can
be calculated by CINDER. The shape of the spectra, on the other hand, is
reasonably certain only in proportion to the fraction of the total energy re-
lease that occurs in the 180 nuclides for which ENDF/B-4 contains detailed
spectral data. Figures 1 and 2 show this fraction, for electrons and photons,
respectively, for each of our six cases. The lower part of each figure ap-
plies to fission induced by a fission-neutron spectrum (cases 25F, 28F, and
49F). The upper part displays the ratio of the 14-MeV fraction to the cor-
responding fission-energy fraction (25H/25F, 28H/28F, or 49H/49F). We see
that in general less than 20% of the total energy is in known spectra at 0.1
second after fission (the lowest fraction is less than 3%, for photons in case
28F). The known fraction rises slowly until about 20 seconds after fission
for photons or ~ 40 seconds for electrons, then rises more rapidly until about
1000 seconds, after which it levels off well above 90% for all cases.

It is tempting to assume that all properties of fission-product decay at
early times will vary slowly and smoothly with the mass of the fissioning
nuclide and the energy of the incident neutrons, simply because the number
of fission products is very large. Figures 1 and 2 are our first indication
that this is not true, and we shall see in the rest of this report that var-
iations of up to a factor of two between cases are typical of most quantities
of interest.

Even so, we can make two generalizations about the known-spectrum frac-
tion. First, particularly for beta decay (fig. 1), this fraction is usually
smaller at all decay times for 14-MeV neutrons than for fission-spectrum neu-
trons. Secondly, at early times the data for $^{238}$U are conspicuously deficient,
whereas $^{235}$U is the first to become well-known. Both tendencies are obvious
consequences of the thermal-reactor orientation of the ENDF system.

Figures 3 and 4 show the total particle multiplicity as a function of
decay time for electrons and photons, respectively. One extreme case from
each figure is reproduced in the other to emphasize differences between beta
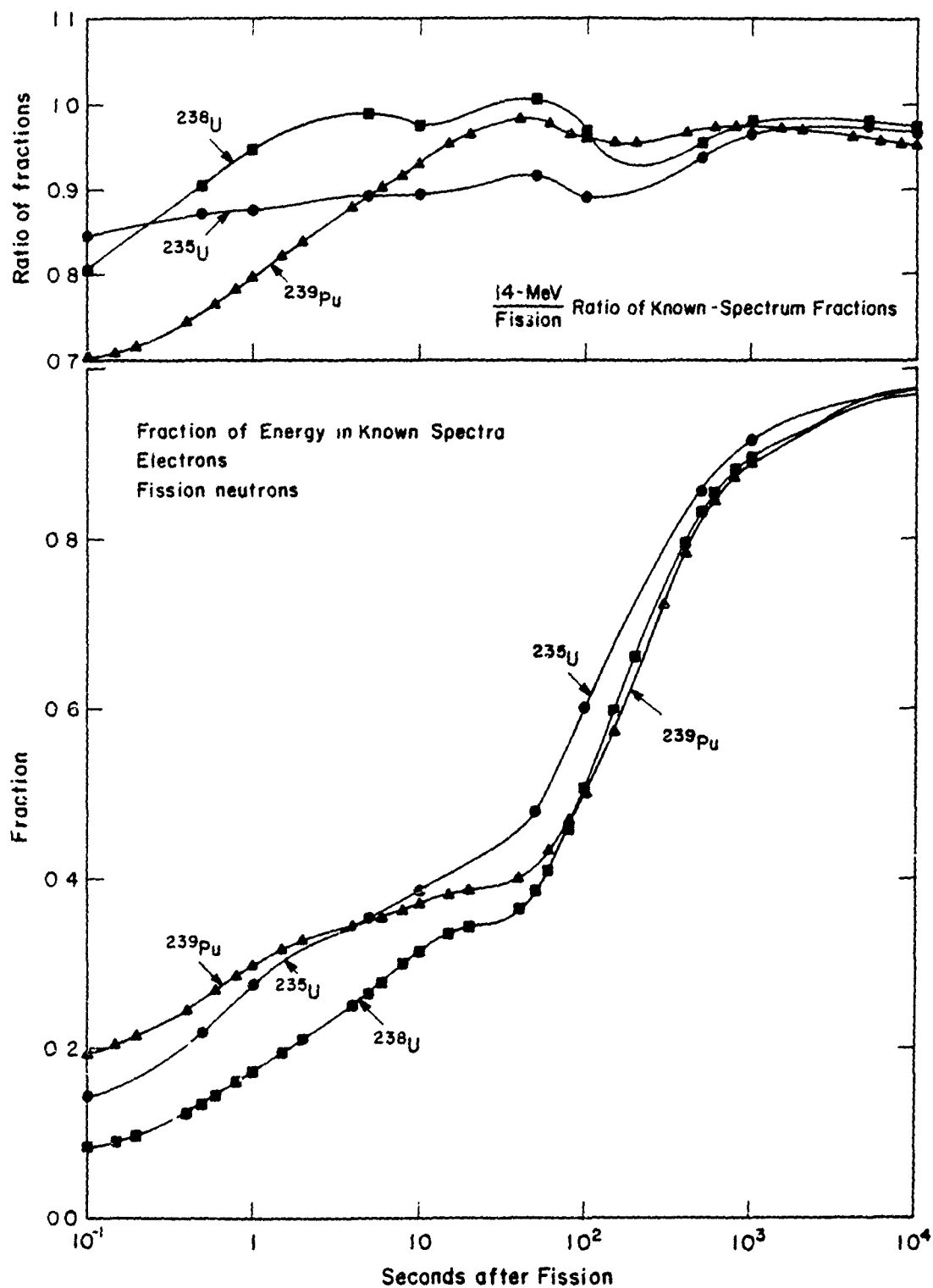and gamma emission. We see that throughout this time range there is more than

13

Figure 1. Fraction of Total Electron Energy, as a Function of Decay
Time, that is Emitted by the 180 Nuclides with Known Spectra.
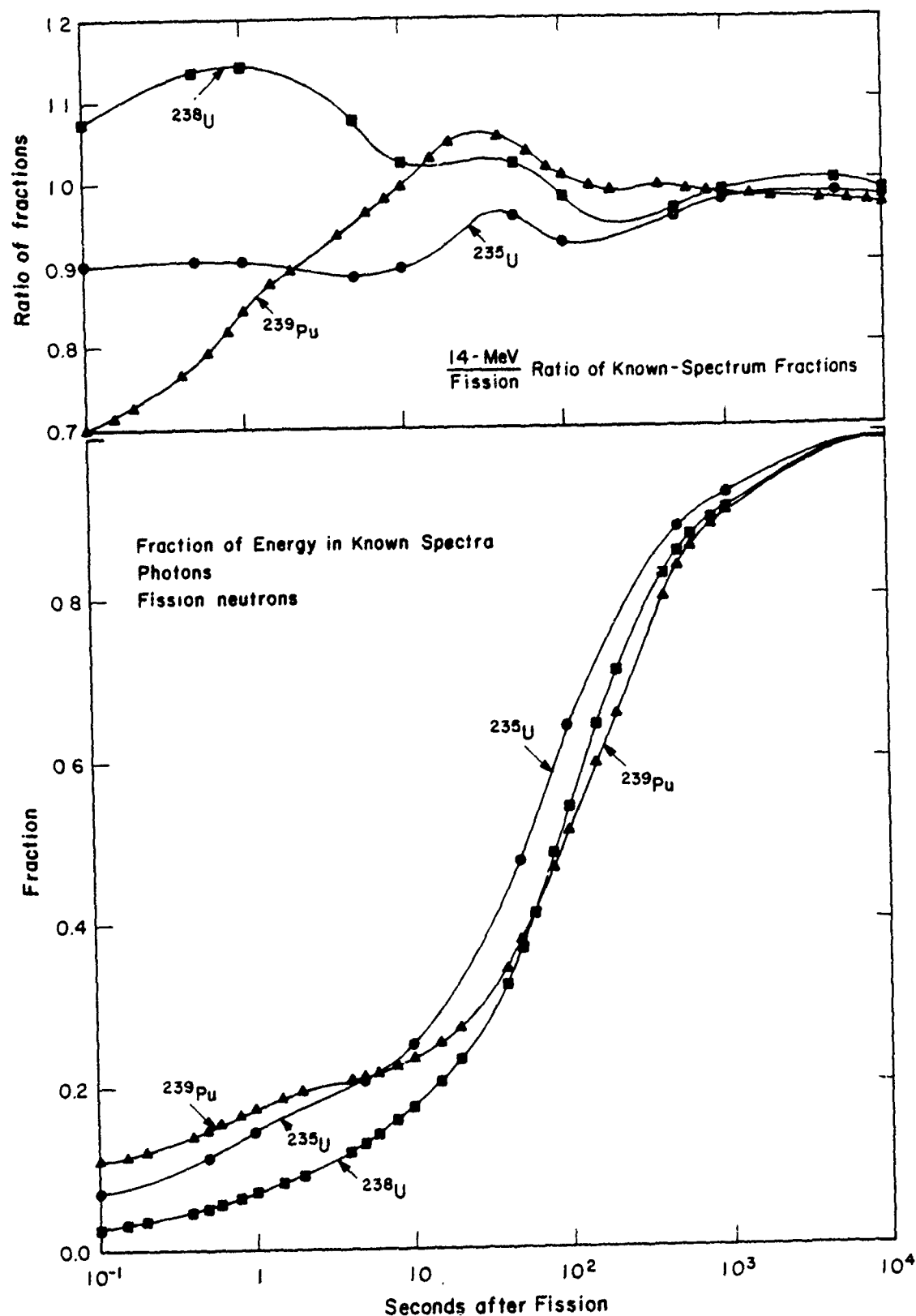Data points are not shown after 1000 seconds.

Figure 2. Fraction of Total Photon Energy, as a Function of Decay Time, that is Emitted by the 180 Nuclides with Known Spectra. Data points are not shown after 1000 seconds.
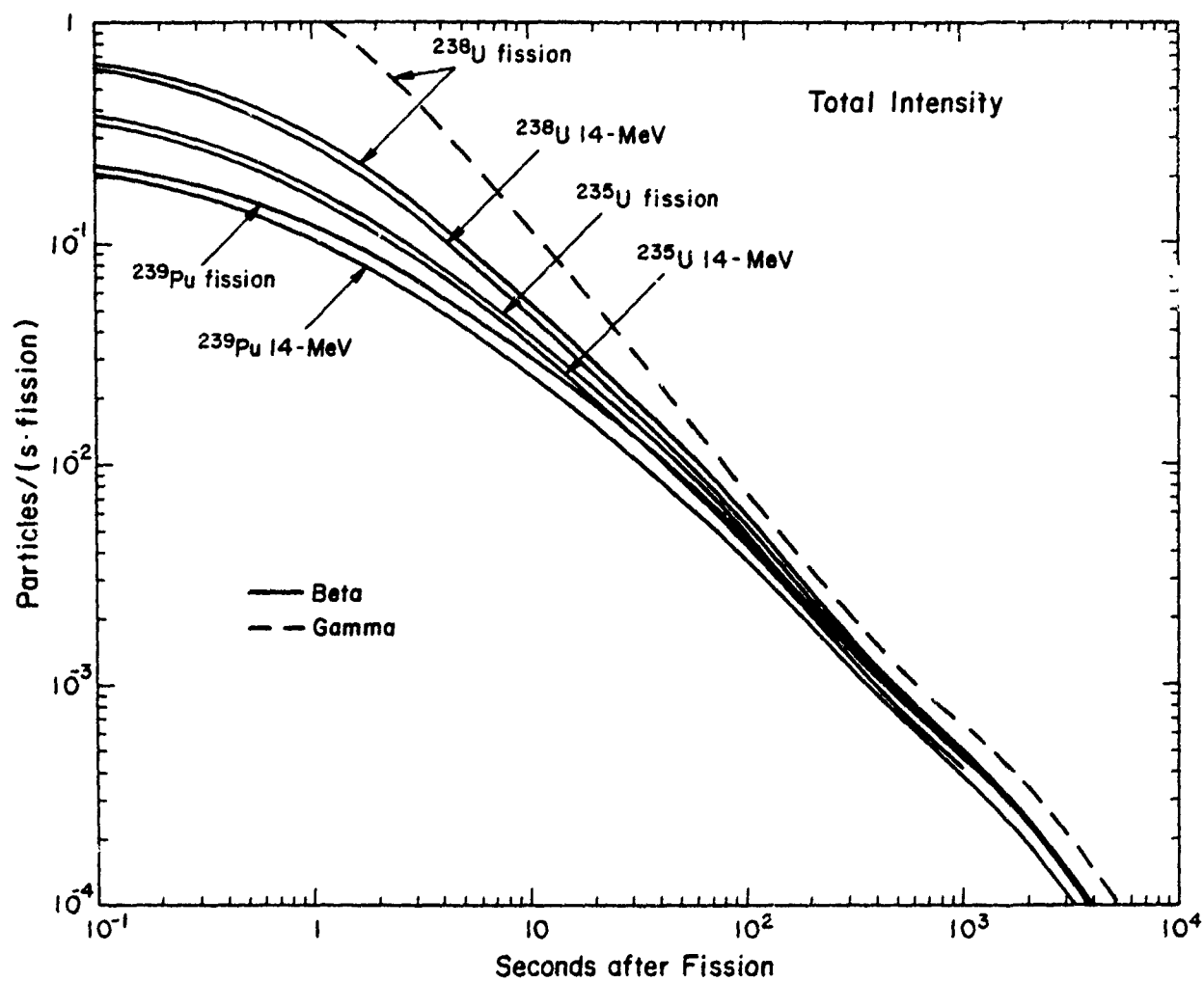
15

Figure 3. Total Intensity of Electrons as a Function of Decay Time.
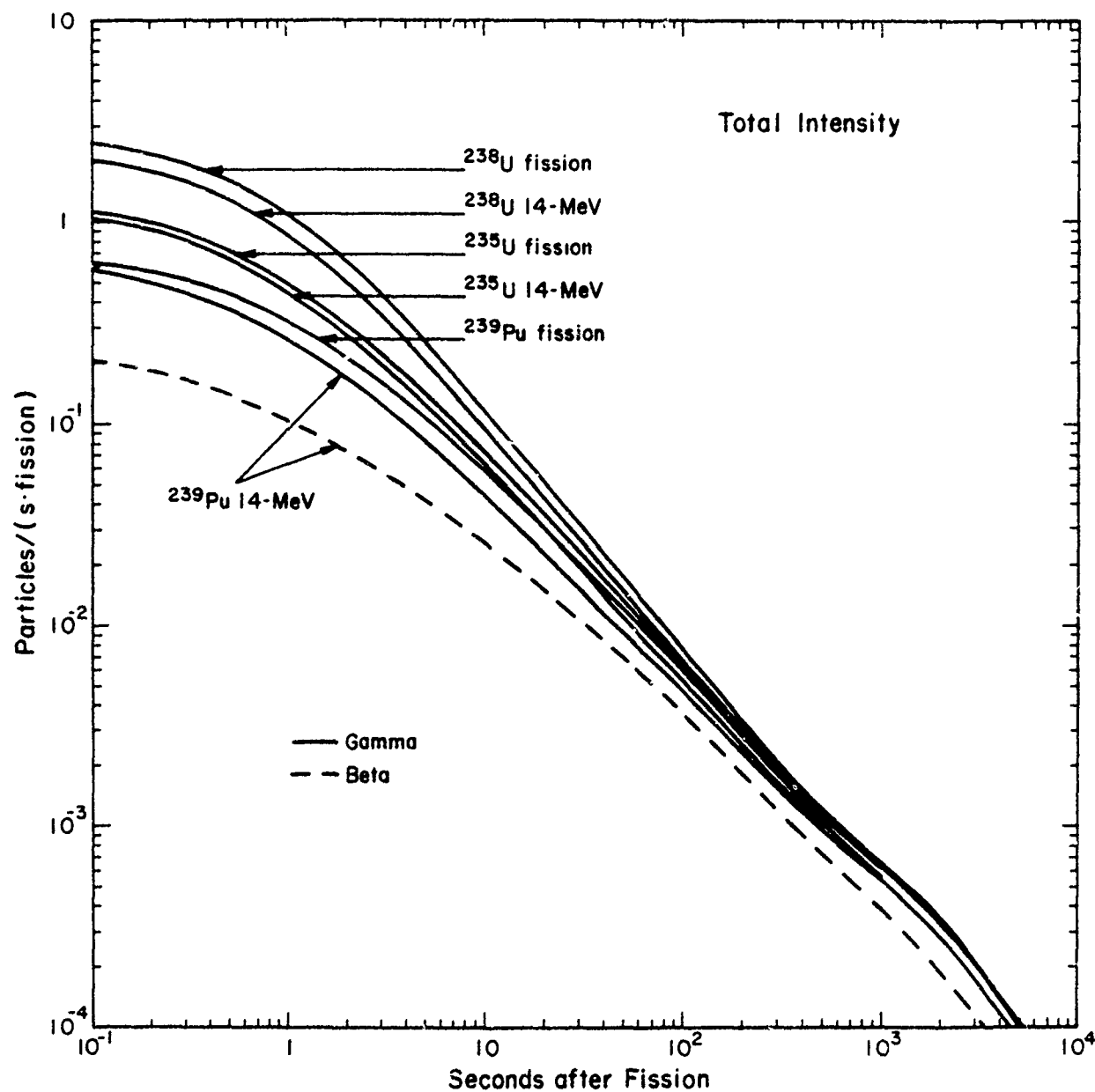One curve for photon decay is included for comparison.

Figure 4. Total Intensity of Photons as a Function of Decay Time.
One curve for electron decay is included for comparison.

17

one photon per electron in all cases, but the relative difference decreases steadily for the first hundred seconds. The total yield of either particle is systematically of the order of 10% less at 14 MeV than for fission neutrons. In both figures the early yield from $^{238}$U is the largest and from $^{239}$Pu the smallest, but the difference is small after 100 seconds. The decay rate for case 49F is markedly smaller than for the other five cases.

In section II we pointed out that the output library from FPSPEC contains absolute emission spectra in 100-keV bins for electrons and 50-keV bins for photons. In order to reduce this information to manageable size, we have rebinned these spectra into group structures appropriate to AFWL's specific needs. Table 3 lists the three structures adopted for this purpose. They

Table 3

AFWL GROUP STRUCTURES FOR FISSION-PRODUCT SPECTRA

| Energy, MeV | 38-gp gamma | 17-gp gamma | 20-gp beta | Energy, MeV | 38-gp gamma | 17-gp gamma | 20-gp beta |
|---|---|---|---|---|---|---|---|
| 7.5 | | | 1 | 1.00 | 19 | 11 | 14 |
| 7.0 | | | 2 | 0.95 | 20 | | |
| 6.5 | | | 3 | .90 | 21 | | |
| 6.25 | 1 | 1 | | .85 | 22 | | |
| 6.0 | | | 4 | .80 | 23 | | |
| 5.5 | 2 | 2 | 5 | .75 | 24 | 12 | 15 |
| 5.0 | 3 | 3 | 6 | 0.70 | 25 | | |
| 4.5 | 4 | 4 | 7 | .65 | 26 | | |
| 4.0 | 5 | 5 | 8 | .60 | 27 | | |
| 3.5 | 6 | 6 | 9 | .55 | 28 | | |
| 3.0 | 7 | 7 | 10 | .50 | 29 | 13 | 16 |
| 2.5 | 8 | 8 | 11 | 0.45 | 30 | | |
| 2.0 | 9 | 9 | 12 | .40 | 31 | | |
| 1.9 | 10 | | | .35 | 32 | | |
| 1.8 | 11 | | | .30 | 33 | | |
| 1.7 | 12 | | | .25 | 34 | 14 | 17 |
| 1.6 | 13 | | | | | | |
| 1.5 | 14 | 10 | 13 | 0.20 | 35 | | |
| 1.4 | 15 | | | .15 | 36 | 15 | 18 |
| 1.3 | 16 | | | .10 | 37 | 16 | 19 |
| 1.2 | 17 | | | .05 | 38 | 17 | 20 |
| 1.1 | 18 | | | .00 | -- | -- | -- |

consist of a coarse-group structure for both electrons and photons and a
compatible second fine-group structure for photons. We shall use these group
structures to display a sampling of the behavior of the spectra.

Figure 5 shows 20-group electron spectra for the 25F case, taken at even
powers to ten from 0.1 to $10^4$ seconds after fission. The early spectrum has a
maximum near 2 MeV that is roughly a factor of 5 greater than the intensity in
the lowest-energy bin. The spectrum cuts off arbitrarily at 7.5 MeV, where the
original binning for the 180 known spectra ends in FPDCYS (ref. 7). The inten-
sity at the cutoff energy is approximately 1% of the maximum at 0.1 second and
decreases rapidly at later times. At later times the maximum moves towards
lower energies and the high-energy part of the spectrum drops more steeply.
After $10^3$ seconds the peak disappears altogether, leaving only the monotonic
decrease with energy.

The corresponding 38-group photon spectra for 25F appear in fig. 6. Here
the individual lines produce such large fluctuations that it is difficult to
plot them in a single figure even at time intervals of a factor of ten. In-
deed, we have had to omit the spectrum at one second after fission. The aver-
age energy of the spectrum at early times is conspicuously lower than for
electron emission, with the four highest peaks all below 1 MeV and a sharp
drop in intensity above 1.5 MeV. The early intensity in the lowest-energy
bin is a factor of a thousand lower than in the first peak, but this extreme
difference disappears after ten seconds. By 100 seconds after fission a broad
background is evident under much-reduced fine structure, with a maximum near
0.6 MeV. The high-energy tail of the spectrum is quite flat at early times,
but, as in the electron spectrum, becomes much steeper at later times. Note
that ENDF/B does not list any photons more energetic than 6.25 MeV.

The densities of many individual fission-product nuclides exhibit growth
followed by decay, but in the electron spectrum summed over all the nuclides
none of the 100-keV bins exhibits growth. On the other hand, because they
are easily dominated by one nuclide many of the 50-keV photon bins do exhibit
a maximum in the decay curve. Figure 7 shows an example; namely, the 50-to-
100 keV bin for case 49F. The same bin in the electron spectrum has no cor-
responding maximum. In contrast to the total intensity as shown in figs. 3
and 4, in this bin the photon intensity actually drops below the electron
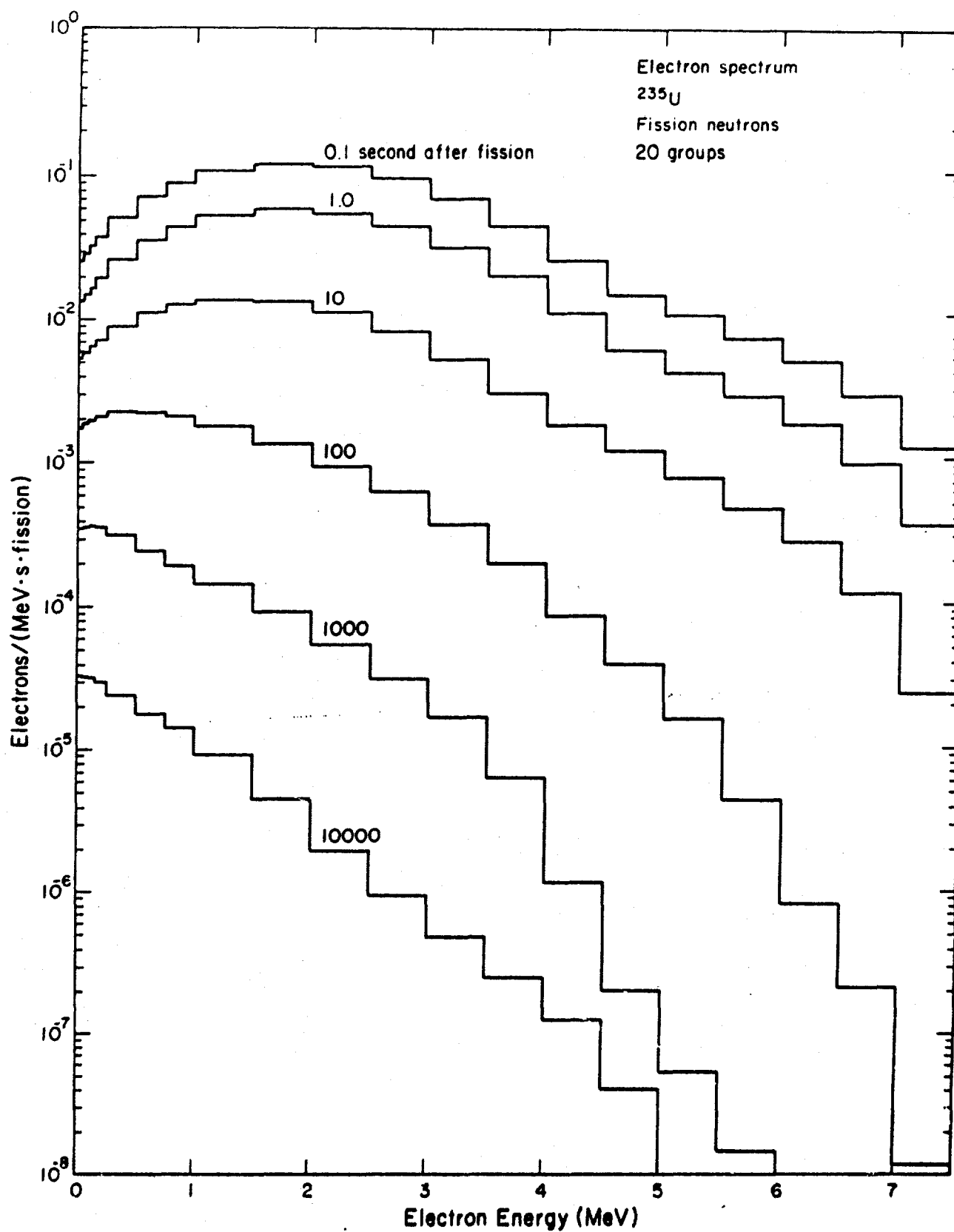intensity after 600 seconds.

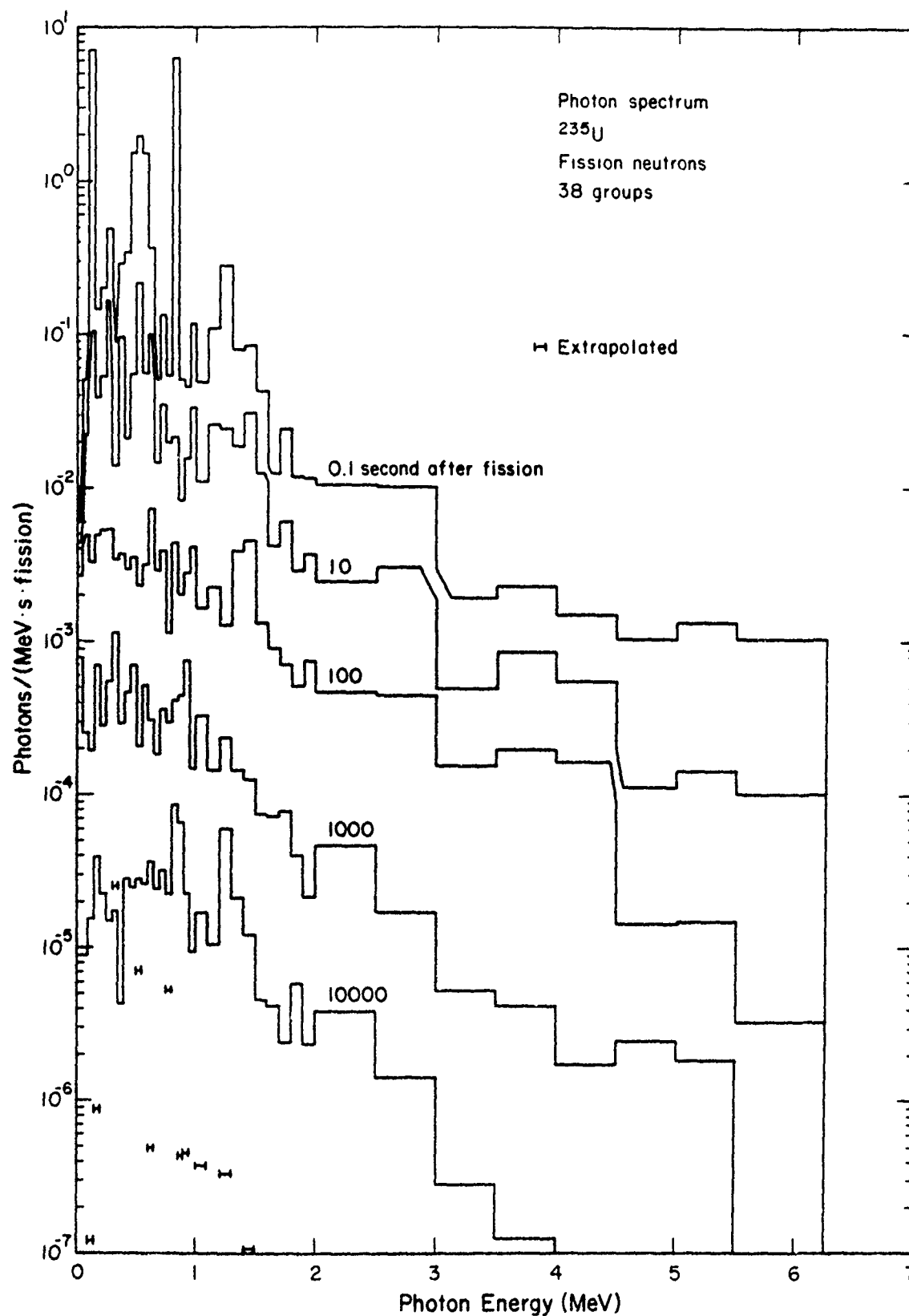Figure 5. Selected 20-Group Electron Spectra Following Fission of $^{235}$U by Fission Neutrons

Figure 6. Selected 38-Group Photon Spectra Following Fission of $^{235}U$ by Fission Neutrons. The "extrapolated" values are discussed in the text.

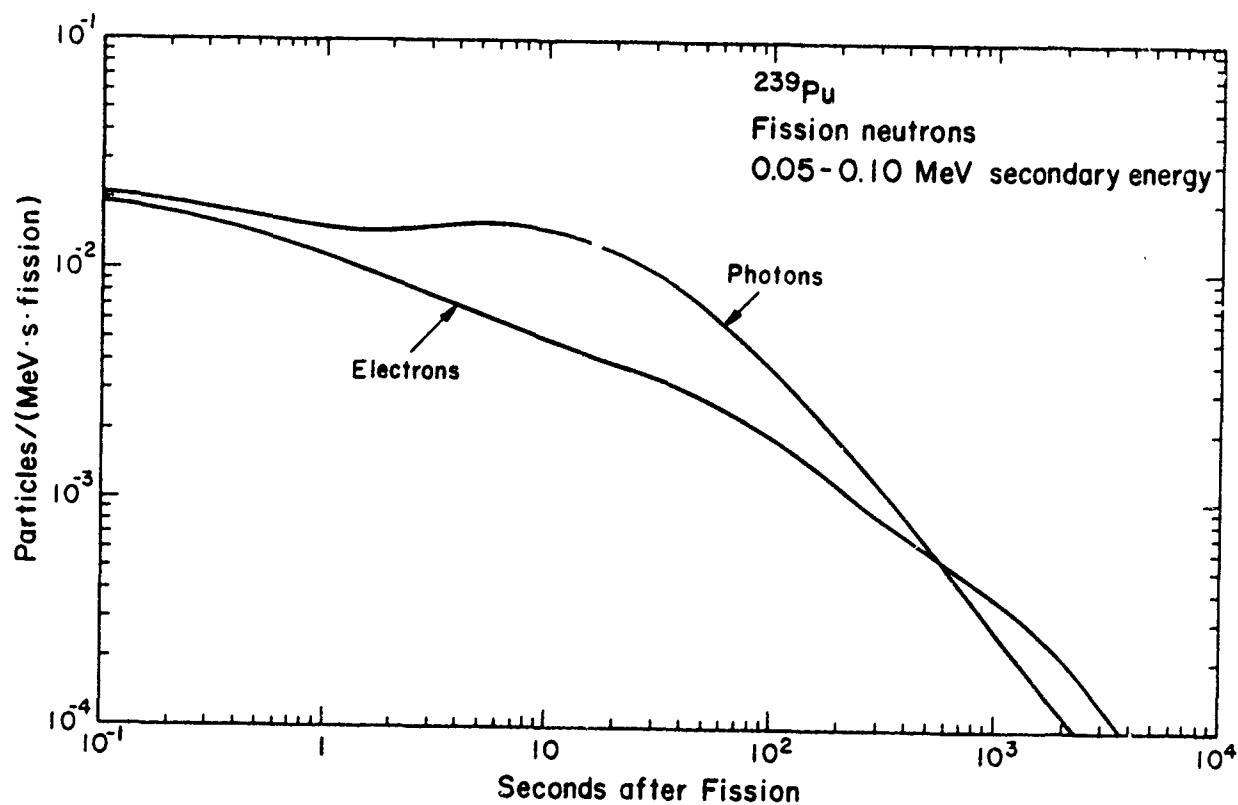Figure 7. Example of Growth Followed by Decay for Low-Energy Photons Following Fission of $^{239}$Pu by Fission Neutrons. Note that growth is not observed for electrons of the same energy.

As a final example of diverse behavior, let us examine the 0.5-to-0.55 MeV bin in the photon spectrum, which is in the center of a peak in the 0.1-second spectrum, and compare it to the broader 0.5-to-0.75 MeV bin in the electron spectrum. In figs. 8 and 9 we see that the photon multiplicity is roughly thirty-fold greater than the electron multiplicity at early times, but decreases very rapidly and crosses the electron decay curve twice in the first thousand seconds. The slower decay in case 49F, which we pointed out in figs. 3 and 4, is especially marked in fig. 9. These two figures show only the fission-energy cases. The ratios of the intensities for 14-MeV neutrons to those for fission neutrons are shown in the two parts of fig. 10. The variations in the electron intensities are comparable to those that we observe in the total intensity. The 14-MeV/fission ratio for the narrow photon bin, on the other hand, shows large fluctuations for all three fissioning nuclei (of the order of 30%).
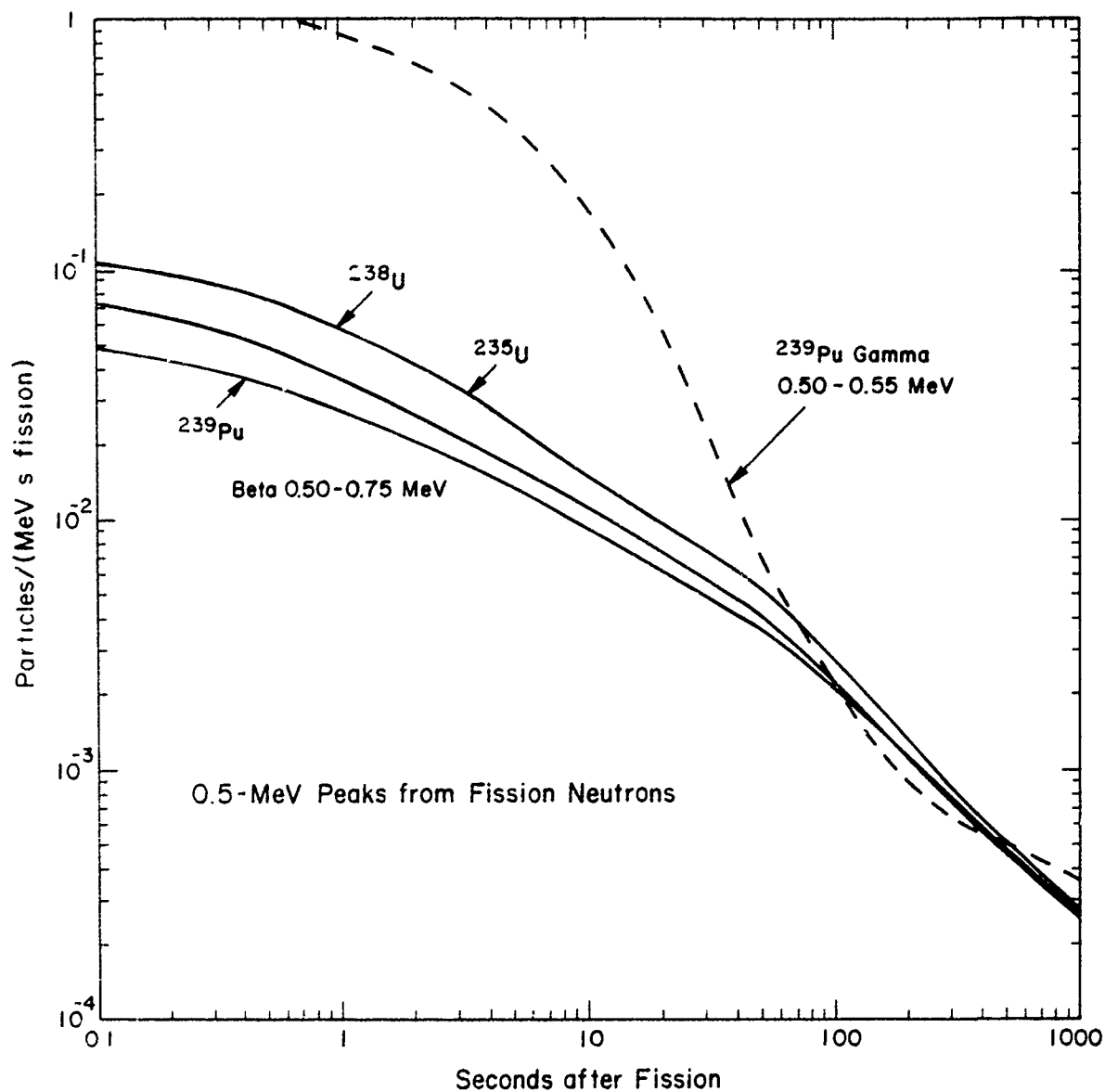
Figure 8.   Decay Curves for a Single Electron Group Following Fission
            Induced by Fission Neutrons.  The dashed line is the corre-
            sponding curve for photons from [239]Pu in the center of the
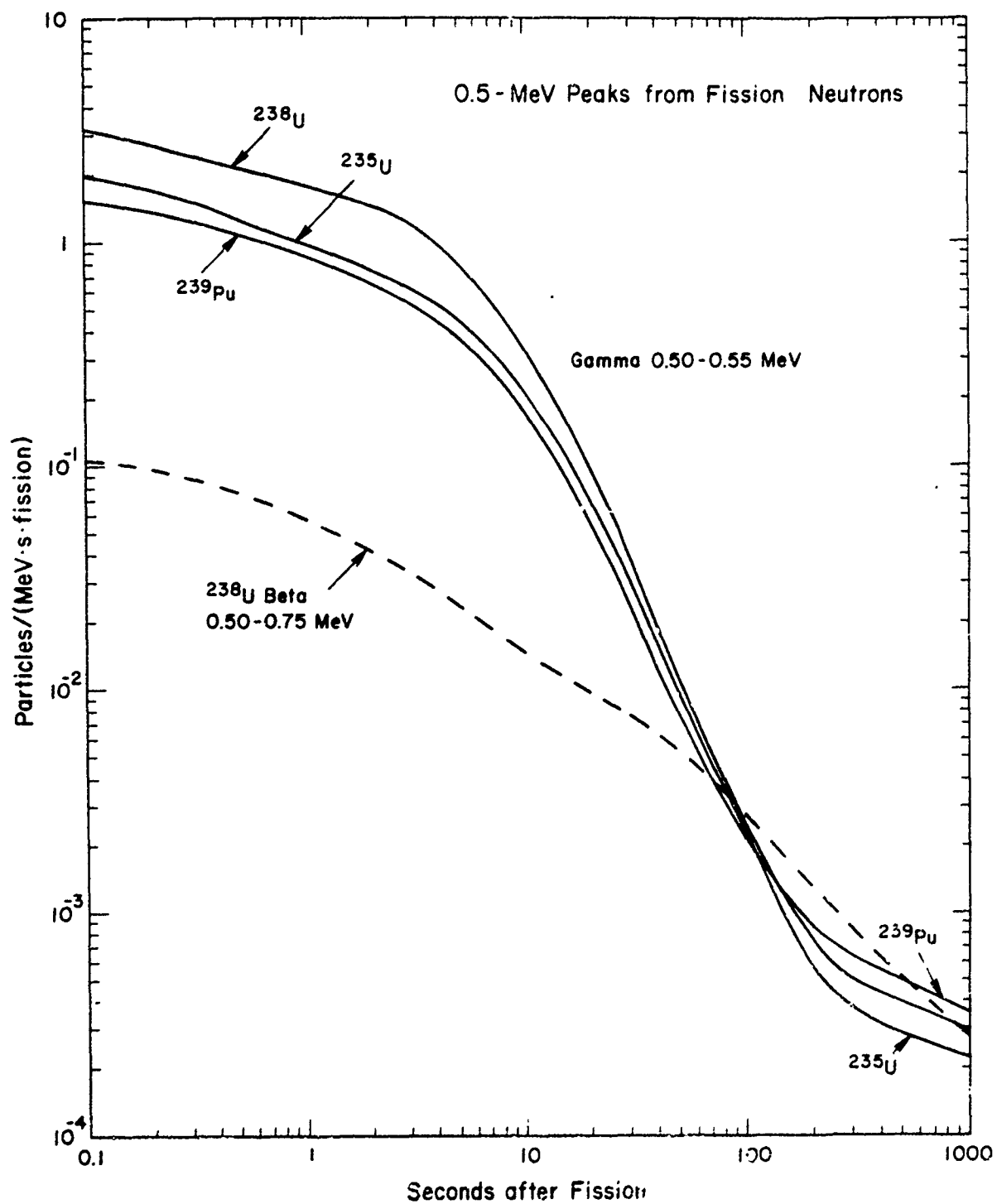            peak at 0.5 Mev.

Figure 9. Decay Curves for a Narrow Photon Group in the Peak at 0.5 MeV, Following Fission Induced by Fission Neutrons. The dashed line is the corresponding curve for electrons from $^{238}U$ at a similar energy.
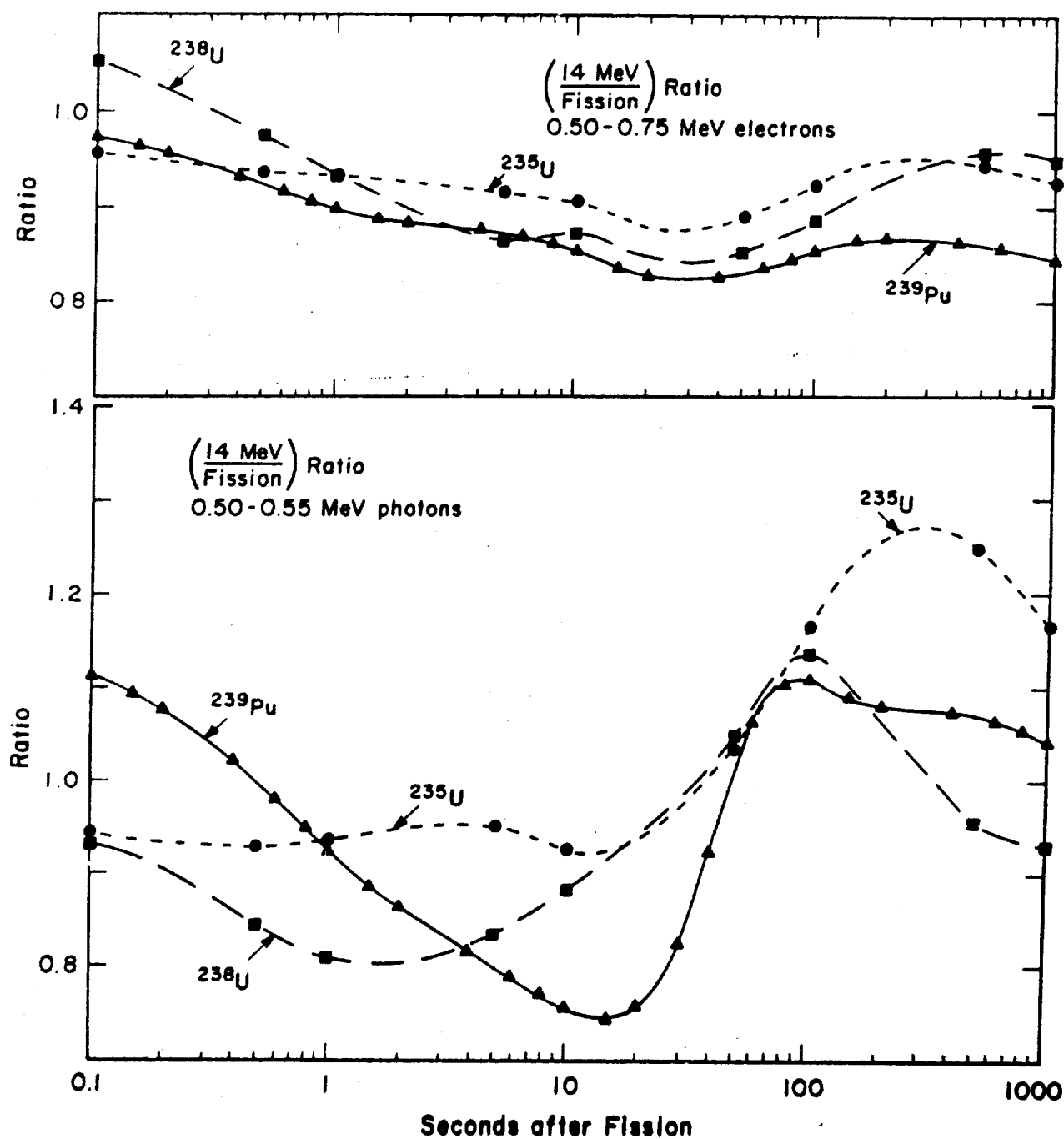
25

**Figure 10.** Ratios of the Decay Curves for Fission Induced by 14-MeV Neutrons to those Induced by Fission Neutrons Shown in Figs. 8 and 9

# SECTION IV

## VALIDATION OF DATA

As with the data themselves, validation of ENDF/B-4 fission-product files has emphasized heat production following $^{235}$U fission induced by thermal neutrons (ref. 9). A number of spectrum benchmarks exist (discussed in ref. 10), but all of them are likewise for thermal neutrons. Nevertheless, it is possible to make some estimates for other fissioning nuclides and other energies.

Schmittroth and Schenter (ref. 11) have propagated the experimental and modeling uncertainties underlying the ENDF/B data through the summation calculations in order to estimate the *a priori* uncertainties in the total energy-emission rate. Table 4 shows part of their results (excerpted from ref. 12) for thermal neutrons incident on $^{235}$U (case 25T), as well as for our cases 28F and 49F. The same authors (ref. 13) have performed a least-squares analysis of the decay-heat benchmark measurements in order to derive *a posteriori* estimates of the same uncertainties, and we have included their results for 25T in table 4. The dominant uncertainties in the ENDF/B data come from the nuclide-yield model, and at early times from the mass-excess estimates for nuclides far from stability. We see from the table that the *a priori* uncertainties are similar for all cases. However, for 25T the *a posteriori* uncertainties are dramatically smaller for decay times between 2 and $10^6$ seconds. Indeed, they turn out to be dominated by systematic disagreements among the thermal benchmarks.

The thermal-neutron benchmarks include a beta-spectrum measurement made at the University of Illinois (ref. 14) following a 15-ms pulse and a gamma-spectrum measurement made at the Oak Ridge National Laboratory (ref. 15) following a 1-s pulse, both of which constitute stringent tests of the short-half-life data. The Illinois measurement agrees very well with ENDF/B-4 after 100 seconds. At shorter decay times and electron energies greater than 0.5 MeV, beta-spectrum measurements from the two laboratories disagree (ref. 12) with each other by amounts comparable to their disagreement with the summation calculations. The Oak Ridge gamma-spectrum measurements are in good agreement with our calculations after 50 seconds, except for a narrow peak near 0.4 MeV, which we systematically underestimate by as much as a factor of two between 20 and 200 seconds after fission.

27

Table 4

PERCENT UNCERTAINTIES IN ENERGY-EMISSION RATE FOLLOWING A FISSION BURST*

| Decay Time, s | $^{235}U$, Thermal neutrons | | $^{238}U$, Fission neutrons | $^{239}Pu$, Fission neutrons |
|---|---|---|---|---|
| | Est.** | Meas.*** | Est.** | Est.** |
| 0.0 | 24.0 | | 32.1 | 42.5 |
| 0.1 | 23.2 | | 31.4 | 42.3 |
| 0.2 | 21.9 | | 28.2 | 38.2 |
| 0.5 | 20.1 | | 24.7 | 32.2 |
| 1.0 | 18.6 | 28. | 22.4 | 27.2 |
| 2.0 | 17.4 | 8. | 20.7 | 22.5 |
| 5.0 | 16.2 | | 19.1 | 18.8 |
| 10.0 | 15.1 | 2.5 | 17.7 | 17.1 |
| 20.0 | 13.6 | 2.1 | 16.3 | 15.6 |
| 50.0 | 10.1 | | 13.4 | 12.8 |
| $1 \times 10^2$ | 6.8 | 1.7 | 9.6 | 9.8 |
| $2 \times 10^2$ | 5.1 | | 6.6 | 7.2 |
| $5 \times 10^2$ | 4.8 | | 5.3 | 5.8 |
| $1 \times 10^3$ | 4.6 | 1.7 | 4.7 | 5.5 |
| $2 \times 10^3$ | 4.4 | | 4.5 | 5.6 |
| $5 \times 10^3$ | 4.3 | | 4.5 | 6.2 |
| $1 \times 10^4$ | 4.3 | 1.6 | 4.7 | 5.9 |
| $2 \times 10^4$ | 3.7 | | 4.1 | 4.6 |
| $5 \times 10^4$ | 3.2 | | 3.5 | 3.9 |
| $1 \times 10^5$ | 3.2 | 1.7 | 3.3 | 3.7 |
| $2 \times 10^5$ | 2.3 | | 2.4 | 3.0 |
| $5 \times 10^5$ | 1.7 | | 2.0 | 2.4 |
| $1 \times 10^6$ | 1.5 | 2.0 | 1.8 | 2.0 |
| $1 \times 10^7$ | 1.6 | 2.0 | 2.1 | 1.9 |
| $1 \times 10^8$ | 2.2 | 2.0 | 3.8 | 3.8 |

\*    Excerpted from ref. 12.
\*\*   Uncertainty estimated by propagating ENDF/B uncertainties to derived
      emission rate.
\*\*\*  Uncertainty deduced from least-squares analysis of benchmark measure-
      ments.

From the above considerations, we estimate that our calculated spectra are about as accurate as present-day direct measurements for decay times for which more than half of the yield comes from the 180 nuclides for which we have spectra in ENDF/B. From figs. 1 and 2 we see that this threshold varies between 50 and 100 seconds after fission. The accuracy of our detailed spectra at earlier times depends on the postulated similarity of the overall spectrum to that of the 180 nuclides, so that for the present we know only that it is no better than the examples shown in reference 10 (see particularly their figs. 52 to 62 and 91 to 94). Our total energy-emission rates are probably correct to substantially better than 5% for decay times greater than 10 seconds.

## SECTION V

## COMPARISON WITH EARLIER CALCULATIONS

For many years the calculations begun by Stovall (ref. 1) and improved by Dieckhoner (ref. 2) have been the standard reference for fission-product spectra cited in calculations for the Air Force. We have pointed out in Section I that the LASL calculations are basically a modern incarnation of the same computational approach. The LASL fission-product work includes a number of improvements in addition to incorporating the results of post-1963 experimental work.

Dieckhoner used 83 mass-chain yields taken from smooth curves, whereas ENDF/B uses actual measurements for 95 mass chains with all irregularities included. ENDF/B uses an empirical model similar to the equal-charge-displacement hypothesis that he used for calculating unmeasured direct yields. In Version 5 (which we have used only for case 49H), ENDF/B adopts two new models (refs. 4 and 5), one to include pairing effects for individual yields within a given mass chain, and another to describe the branching ratio between ground and isomeric states (which normally strongly favors the isomer, contrary to the previous common assumption). Dieckhoner's longest linearized chains contained only 10 members, whereas CINDER uses up to 20 and includes interchain transitions that result from neutron capture and emission. Also, CINDER uses a single general solution to the linearized-chain differential equations, rather than special forms for each length of chain. We have also given exhaustive attention to the problem of numerical stability of the solutions, which Dieckhoner does not seem to have addressed at all, but which we now know can cause order-of-magnitude errors. Furthermore, instead of estimating the spectrum from average ratios of beta end-point energy to total decay energy, we have used exact spectra of 180 dominant nuclides as models. Finally, we have added the data required to generate photon decay curves to those required for electrons.

CINDER includes the detailed treatment of irradiation history recommended by Dieckhoner, so that it can follow neutron-induced changes in fission-product concentrations. However, in the absence of such transmutation it is not necessary to have this ability in order to correct for either finite irradiation time or finite counting time. LaBauve, *et al*, point out in ref. 16 that it

should be possible to use the results of a fit such as we shall describe in Section VI to transform the results of a short-burst calculation analytically into the result for any specified finite irradiation and counting times.

Only one of Dieckhoner's four cases corresponds directly to one of ours; namely, the electron spectrum for case 25F. Two of his other cases are for thermal neutrons, which have negligible effect in practical nuclear explosions, and the fourth is a "thermonuclear" case which contains an unspecified mixture of isotopes and neutron energies.

Figure 11 compares Dieckhoner's 25F case with our calculations, which have been interpolated to his decay times by using the fits described in Section VI. As one would expect from the paucity of measurements for short half-lives, his calculations have missed about half of the intensity extrapolated back to zero time. He also had serious difficulty with the high-energy part of the spectrum, which at 7 MeV he underestimated by an order of magnitude for 0 through 20 seconds and overestimated by factors of 10 to 40 between 60 and 300 seconds. On the other hand, his calculations at 2, 6, and 10 seconds agree with ours within about 10% from zero to the maximum in the curve, and the 2-second curve is still less than 25% low at 5 MeV. After 20 seconds his calculations are about a factor of 2 low at zero energy, but all of them cross our curves near 4 MeV and end up much higher at 7 MeV. The 300-second curve agrees with ours within about 15% from 0.5 to 4 MeV. At 1 MeV, all of his curves except the one at 0 seconds agree with ours within 30%, but 5 out of these 7 are low.

31
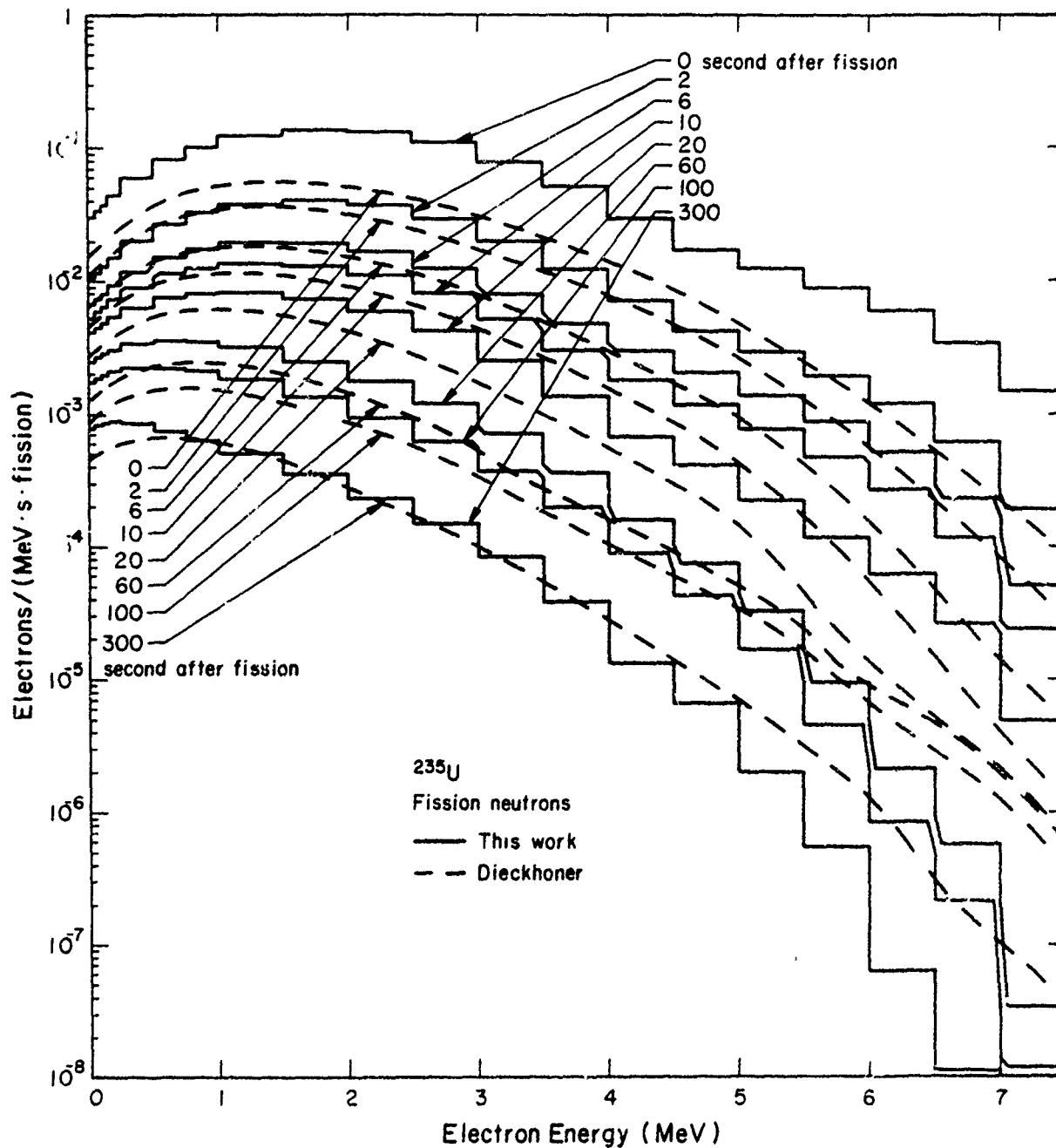
Figure 11.  Comparison of the Results of the Present Work with those of
            Dieckhoner (Ref. 2).  The spectra are for electrons follow-
            ing fission of $^{235}U$ by fission neutrons.  The 20-group
            spectra from this work at decay times of 10 and 100 seconds
            are also plotted in fig. 5.

## SECTION VI

## PREPARATION OF COMPACT PARAMETER SET

### 1. FITTING ALGORITHM

One obvious method for representing a multigroup spectrum of fission-product radiation as a function of time is to perform a least-squares fit of each group to an exponential series of the form

$$y_g = \sum_{i=1}^{m} \alpha_{gi} \, e^{-\lambda_{gi} t} \, , \tag{1}$$

where $y_g$ is the intensity in group g at decay-time t and m is the number of terms in the series. Previous work at LASL (ref. 16) has shown that this gives a satisfactory description for the few-group energy-emission rate and the total energy-emission rate. Indeed, a 23-term fit to the total energy has been proposed (refs. 12 and 17) as an engineering standard for reactor use. Our purpose in the present project was to extend this technique to the particle spectra, using finer group structures specified by AFWL.

Our basic tool for the fitting was a Fortran program called FPSPFT that was written specifically for this purpose and run on a CDC-7600 computer under the Chili Ridge Operating System (CROS). The input data were prepared under CROS by FPSPEC as we have already described in Section II. We had anticipated difficulty in fitting the gamma spectrum because it exhibits growth followed by decay, as illustrated in fig. 7. This specific problem did not materialize, but on the other hand we had much more difficulty in all of the fits than we had anticipated.

The fits are all weighted* so as to define $\chi^2$ in terms of the <u>relative</u> error at each decay time. We ignore the overwhelming covariance introduced by the CINDER calculation and use a diagonal weight matrix. We find that the design matrix is linear with respect to the amplitudes $\alpha_{gi}$ but nonlinear with respect to the decay constants $\lambda_{gi}$.

---

*Mathematical details of the fitting process are summarized in appendix A.

The nonlinear nature of the fit implies that there may be more than one relative minimum in $\chi^2$, which we find to be a pervasive problem for more than three terms in the fit. Because of the large number of groups to be fitted, we made the search for absolute minima a largely automatic process that is built into FPSPFT. We shall outline the automatic procedure here and discuss it in more detail in appendix A. As we shall see in Section VI.3, however, the automatic search proved inadequate for fitting the photon spectra, so that we were forced to adopt additional nonautomatic measures to obtain acceptable fits.

The automatic search in FPSPFT is conducted on two levels. Every fit begins with a trial set of decay constants, from which a straightforward calculation gives the corresponding amplitudes for an absolute minimum in $\chi^2$. The complete parameter set is then iterated, following the multidimensional gradient of $\chi^2$, until it either converges to a relative minimum or else clearly fails to converge at all. The central problem, then, is to find a trial set of decay constants that lies close enough to the optimal set for the initial gradient to guide the solution to it.

In order to explore parameter space reasonably thoroughly, FPSPFT uses up to six different trial sets. The fitting algorithm always starts with the lowest-energy group. Once a group has been fitted, its parameters are used as the first guess for the next higher group. This guess is almost always successful for the smooth electron spectrum, at least in the sense that it finds a corresponding relative minimum (whether or not that proves to be an absolute minimum). It frequently fails for groups near the high-energy end of the electron spectrum, however, and usually fails for the much more irregular photon spectrum.

The second obvious estimate is found by making an empirical search for regions of the decay curve that appear to be dominated by a single decay constant. At late decay times in the highest-energy groups the decay is frequently dominated by a single isotope, so this procedure is often fruitful. For the dense data sets the search is made by fitting a five-term Lagrange interpolating polynomial to the logarithm of the group intensity and examining the derivatives of that polynomial. For the sparse data sets this fit is too erratic to be useful, and the empirical search cannot be used.

Four other trial sets are based on the apparent decay constants at the beginning and end of the time interval that is being fitted. For the dense

34

sets these are taken from the Lagrange fits. For the sparse sets the logarithmic slopes between the first two and the last two points are used instead, with an optional[*] procedure to extrapolate the estimate averaged over the last interval to the latest time in that interval. The four trial sets are then formed by using various systematic subdivisions of the interval between these two extreme slopes. In appendix A these are referred to as equispaced subdivisions.

FPSPFT also offers the option of dictating initial estimates of the decay constants from input cards, for selected groups or for all groups. In this event an additional option allows the minimization of $\chi^2$ to be carried out solely by choosing the best amplitudes, or alternatively by iterating on the entire set of parameters.

## 2. PROPERTIES OF INDIVIDUAL FITS

Clearly the effect of increasing the number of terms m in the fit is to allow the fit to follow more of the undulations in the decay curves. Figure 12 illustrates the resulting improvement for the electron spectrum in case 49F. The bottom portion of the figure refers to the same group of electrons that was displayed in figs. 8 and 10. We see that the fit crosses the data at precisely 2m points, as expected, and also that the error nowhere exceeds 5% for $m > 3$. If we sum the fit over all groups and compare the sum to the sum of the input data, we obtain the results in the top portion of the figure. We observe that the errors in the total yield are roughly equal to those in the individual group yields; that is, that no major reduction results from averaging over many groups.

The reason for the latter result should be clear from fig. 13, which shows the error at 10 seconds after fission for each group in the same electron spectrum. There is enough similarity in the shape of the decay curve for each group that many adjacent groups will have errors of the same sign and comparable magnitude at any given decay time. Naturally the locations of the regions of large error depend on the number of terms fitted. Figure 14 shows the corresponding errors for the photon spectrum. Here the errors in adjacent groups are less strongly correlated, but the magnitudes display greater extremes.

---

[*] In Section VI.3 we shall refer to this as the L option.
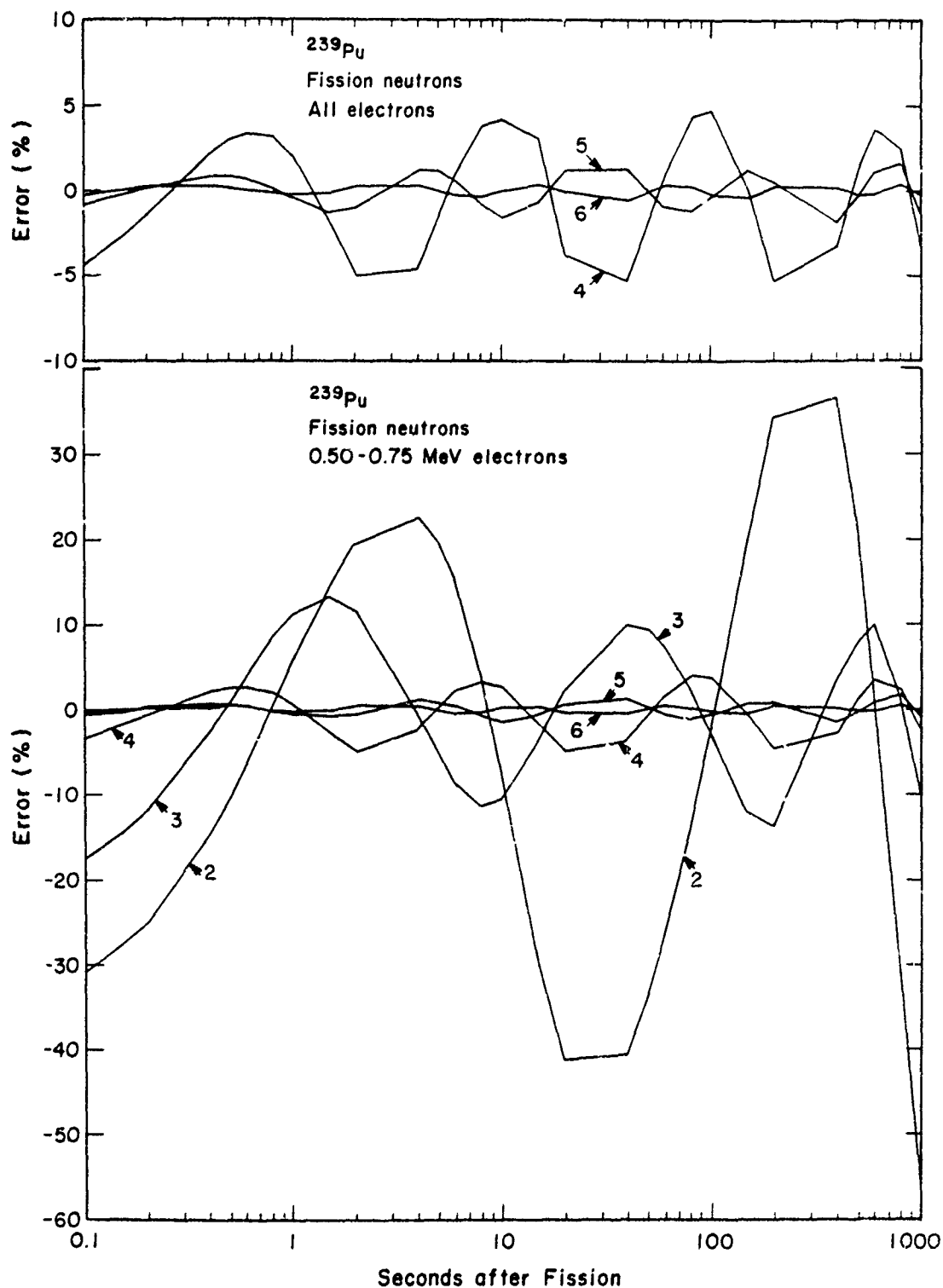
Figure 12. Variation of Fitting Error with Decay Time as a Function of the Number of Terms Fitted (m). This example is for a single group and for the total intensity of electrons emitted by $^{239}$Pu following fission induced by fission neutrons. Each curve is marked with the corresponding value of m.
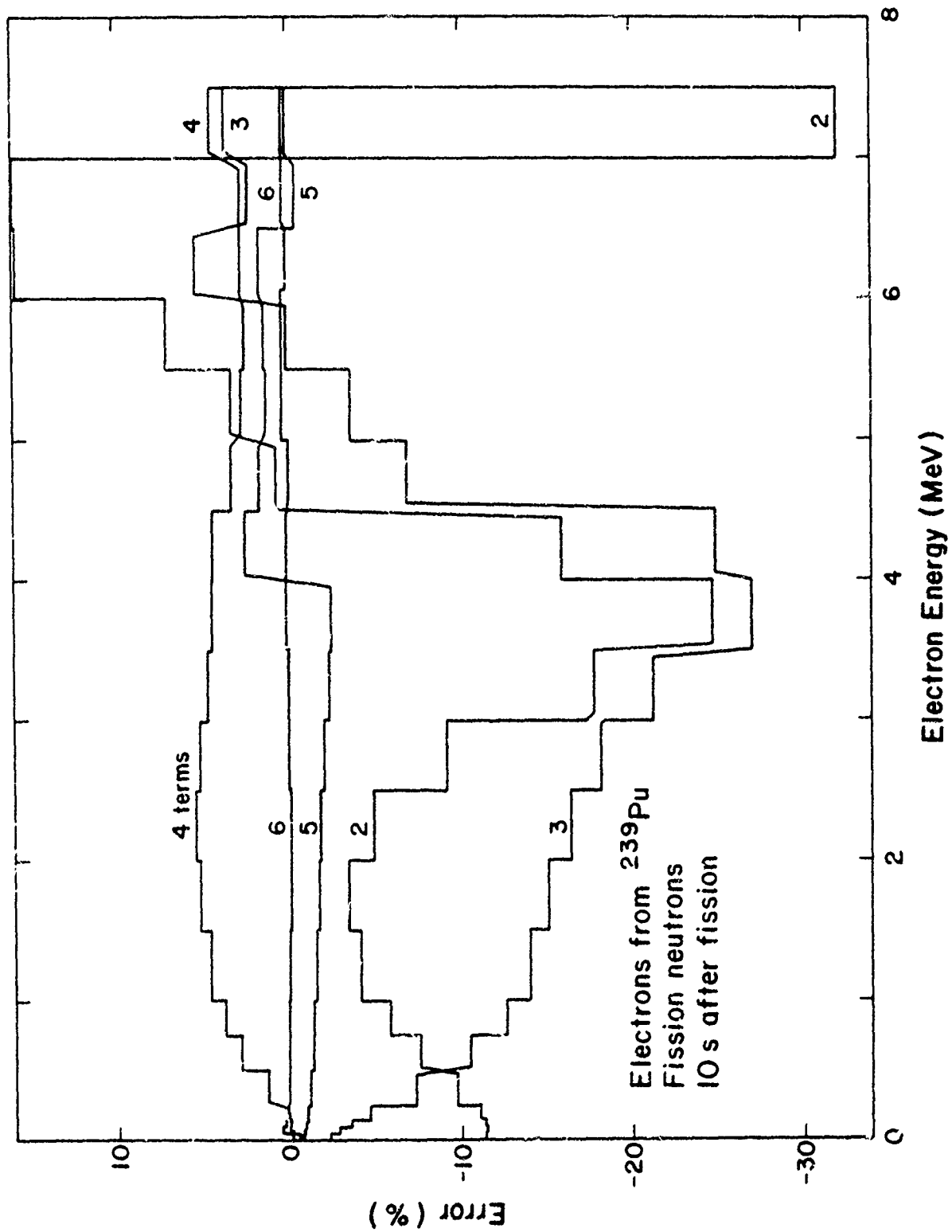
Figure 13. Error in the Fit to the 20-Group Electron Spectrum 10 Seconds after Fission of $^{239}$Pu Induced by Fission Neutrons, as a Function of the Number of Terms in the Fit (m)
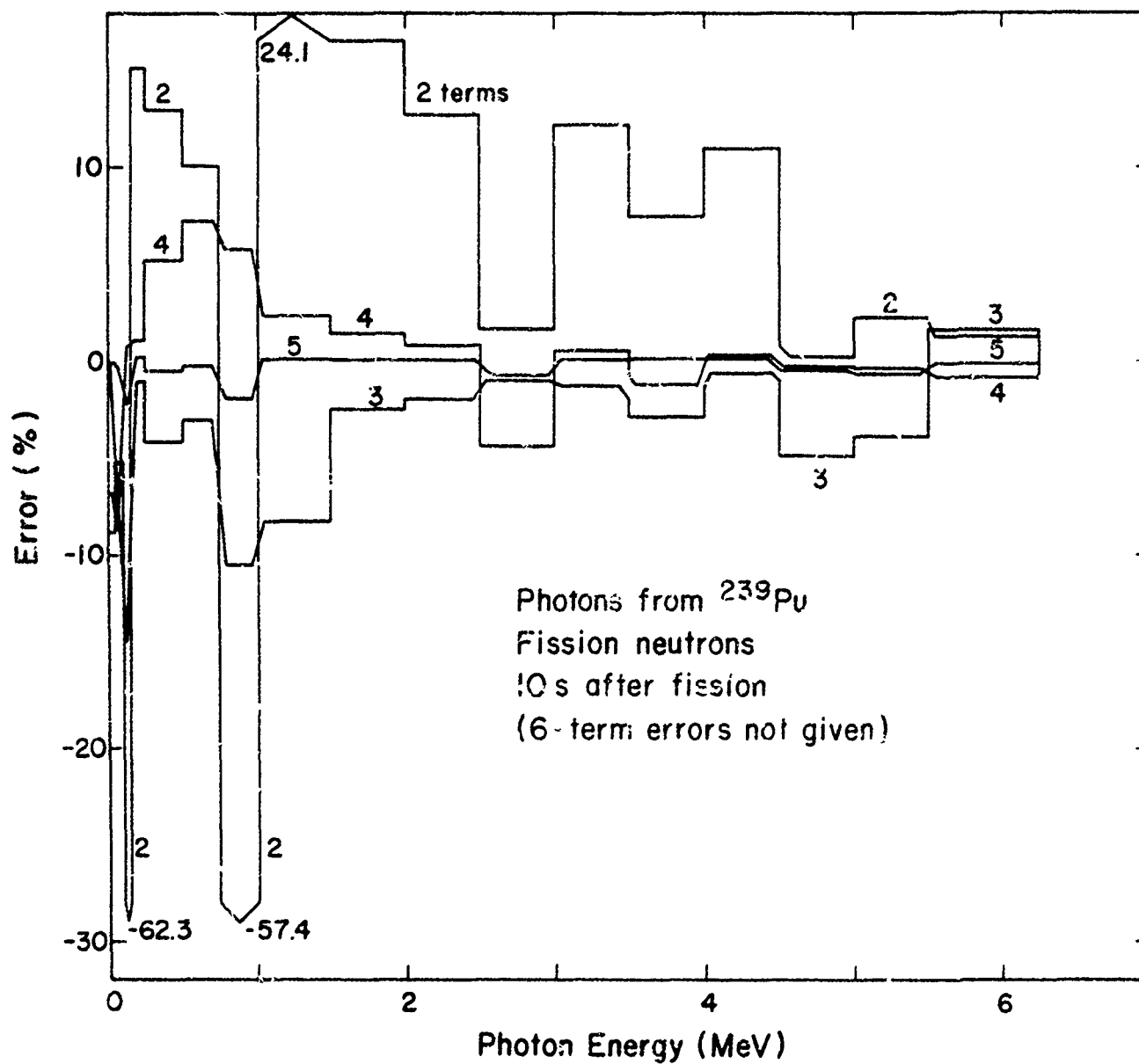
Figure 14. Error in the Fit to the 17-Group Photon Spectrum 10 Seconds after Fission of $^{239}$Pu Induced by Fission Neutrons, as a Function of the Number of Terms in the Fit (m). The error for 6 terms is too small to plot here.

### 3. ADDITIONAL MEASURES TO FIND BEST FITS

The measures that we described in Section VI.1 were developed using the electron spectrum as a test problem. For each of our six cases we punched output cards containing the best parameter sets, and their root-mean-square (rms) errors, for values of m from 2 through 5 (2 through 6 for the dense sets). In a few instances we had to exercize the L option mentioned in Section VI.1 in order to get the best fit.

In an attempt to broaden the search for absolute minima in $\chi^2$, we then used each of these punched parameter sets as the initial estimate for the other five energy-isotope cases, allowing FPSPFT to iterate all parameters from that start. In none of these cases did we find a further improvement in $\chi^2$, which we found to vary smoothly from group to group, so we accept these parameters as giving the best possible fits.

To our dismay, in both the 17- and 38-group photon spectra we found that the L option gave better fits in some groups and worse fits in others. Accordingly, we had to include both alternatives in the cross-fertilization process described above. This time the cross-fertilization produced many improvements in $\chi^2$, some of them very large improvements, especially in the 4- and 5-term fits. Some of these triggered improvements in adjacent groups also. When the improved solutions were recycled into the cross-fertilization they produced still further improvements. This process finally converged after four iterations. It required much clumsy hand work with thousands of cards, so that we were eventually driven to writing a separate computer program just to read and compare the rms-error cards.

### 4. OVERALL FITTING ERRORS

For each case FPSPFT calculates rms relative errors routinely for the fit to each group in a spectrum, for the ensemble of all points in all groups, and for the summed fits compared to the CINDER/FPSPEC sums. In support of our qualitative remarks that are illustrated by figs. 13 and 14, the rms error in the sums is always smaller than that for the ensemble, but usually not very much smaller. For practical purposes in judging the effect of using a particular number of terms in the fit, it is more useful to calculate a yield-weighted rms error, defined as the square root of the weighted average of $\chi^2$, where each group is weighted by its integrated yield from C to $10^3$ seconds. In addition, in compounding these results over our six energy-isotope cases

it is appropriate to weight the dense and sparse cases by the number of times in the case.[*]

The resulting point-and-yield-weighted rms error (PYWE) provides a convenient index for evaluating the penalty associated with using a given number of terms in the fit. The result is plotted as the solid lines in fig. 15. We see that for only two terms the PYWE is about 30% for both electrons and photons regardless of the number of groups in the spectrum. The PYWE is less than 2% for 5 terms and less than 1% for the three cases in which 6 terms can be fitted, although in the latter cases there is more than a factor of 2 spread between the 20-group beta and 38-group gamma PYWEs. Figure 15 in conjunction with the error estimates for the ENDF/B data base discussed in Section IV thus allows an informed choice of how many terms to use for a particular application.

5. EXTRAPOLATION

Fitting a decay curve with an exponential series permits extrapolation to both earlier and later times. Clearly, the fitting process cannot usually pick up components with decay constants whose reciprocals are much smaller than the earliest or much larger than the latest time included in the fit.

There are so few beta-decay half-lives less than 0.1 second that we can be certain that CINDER calculations will extrapolate reliably to zero time. On the basis of the half-lives in ENDF/B we find that less than 1% of the integrated electron yield from zero to infinity occurs before 0.1 second. On the other hand, we have pointed out in Section I that we have deliberately ignored the gamma emission at early times. This emission, which accounts for roughly 45% of the photon emission from zero to infinite time, includes a very intense prompt burst within the first nanosecond followed by decay of more than 60 known activities with half lives between a few ns and 80 µs (ref. 18). The delayed component, which is usually attributed to isomers of the primary fission fragments, becomes negligible relative to the photons following beta decay at a decay time of about a millisecond.

[*] Five terms with two parameters per term permit an exact fit to the 9-point sparse sets in most groups, but the fits are physically unrealistic. Hence we should reduce the weight of the sparse sets.
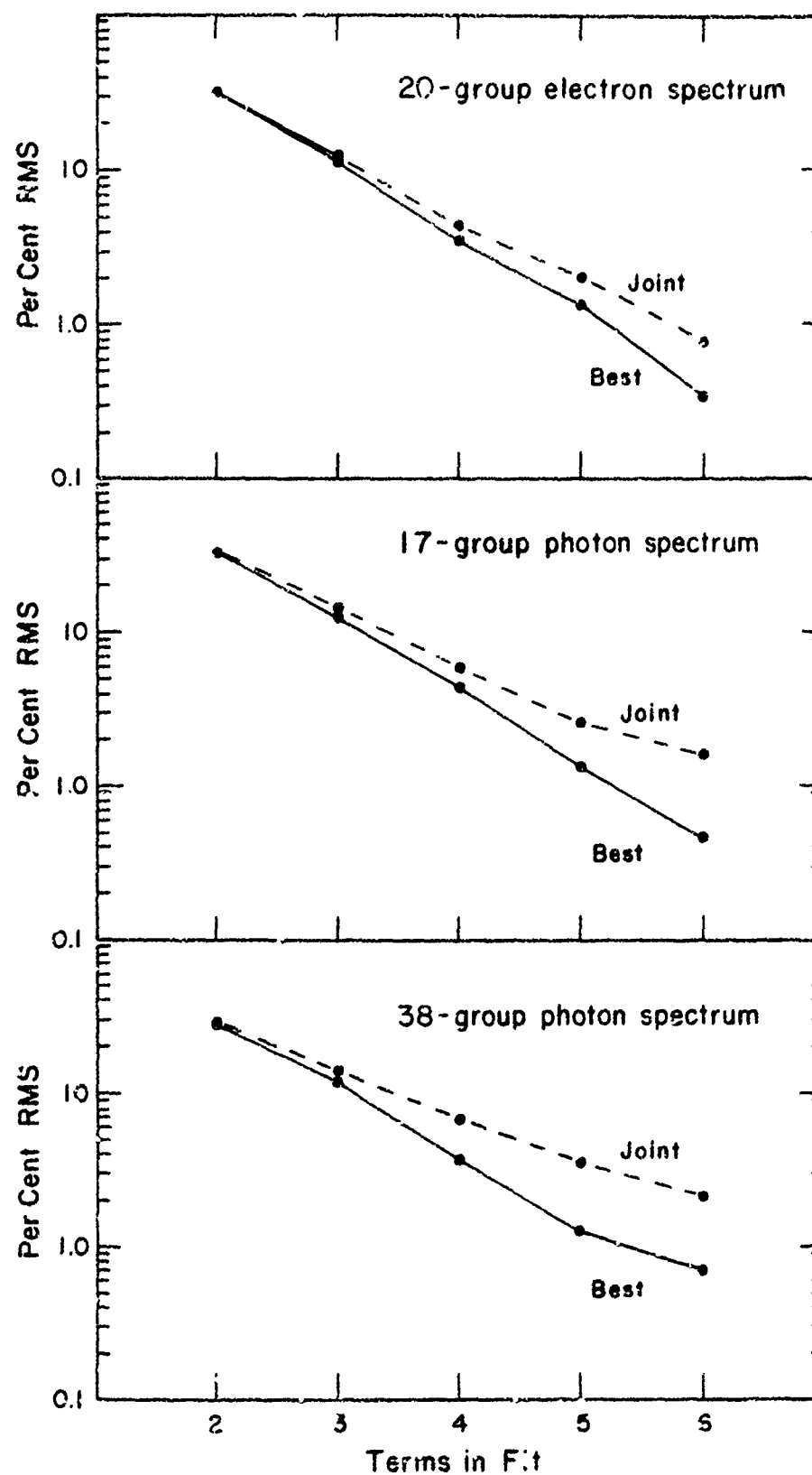
Figure 15. Point-and-Yield-Weighted Root-Mean-Square Error for Independent and Joint Fits to the Six Cases Treated in the Present Work, as a Function of the Number of Terms in the Fit (n)

Since gamma emission more than a thousand seconds after fission is almost entirely from de-excitation of the daughters of beta decay, both emissions should have comparable inaccuracies in extrapolating the total emission to later times. To illustrate such extrapolation, in case 49F our fit from 0.1 to $10^3$ seconds predicts that 84% of the total number of electrons that will be emitted have emerged by $10^3$ seconds, and by extrapolation that 100% will have emerged by $10^4$ seconds. Unfortunately, if we extend the fitting range to $10^4$ seconds we find that only 70% of the emission is actually complete by $10^3$ seconds, 13% more emerges by $10^4$ seconds, and extrapolation beyond $10^4$ seconds predicts at least an additional 5% to infinity.

In fig. 5 we showed selected 20-group electron spectra for case 25F out to $10^4$ seconds after fission. If the fit stops at $10^3$ seconds, no group extrapolates to an intensity at $10^4$ seconds that is greater than the bottom of the figure $[10^{-8}$ electrons/(MeV·s·fission)], although all groups below 5 MeV should exceed that limit. In fig. 6, on the other hand, we see 11 out of 38 photon groups fitted to only $10^3$ seconds that extrapolate to values at $10^4$ seconds that are greater than the bottom of the plot $[10^{-7}$ photons/(MeV·s·fission)], including one that extrapolates to a greater intensity than the correct value from CINDER.

To summarize, roughly 30% of the beta-decay-dominated emission occurs after $10^3$ seconds. The intensities at $10^3$ seconds and integrals up to that time can be represented accurately by parameters fitted from 0.1 to $10^3$ seconds, but extrapolating that fit misses about 5% of the total yield to infinity. The extrapolated intensity is almost invariably too small by at least a factor of ten at $10^4$ seconds, and the error is much more erratic in the photon spectrum than in the electron spectrum.

6.  JOINT FITS

The existence of multiple relative minima in $\chi^2$ suggests that each group in a spectrum might be fitted reasonably accurately by a wide variety of decay constants, as long as the amplitudes are chosen accordingly. This suggests in turn that a single set of decay constants might be used for all six energy-isotope cases simultaneously, thus reducing by nearly a factor of two the total number of parameters required to represent all of the data with a specified accuracy. If such a joint fit is successful, it offers an important but less obvious additional advantage. The sparse data sets are divided very unequally, with time intervals of a factor of five alternating with a factor

of two. We find that the overdetermined 5-term fits to these sets oscillate systematically towards and away from the fits to the dense sets, taking advantage of the factor-of-five gap in which they are unconstrained to make it easy to fit the pairs of points that are only a factor of two apart. Thus, the use of a single set of decay constants (derived in this case only from the dense sets) probably insures a fit that is closer to the true (but uncalculated) values in the long gaps.

We did not recognize the desirability of combined fits soon enough to design simultaneous fitting of many cases into FPSPFT. Accordingly, we tried the simple alternative of averaging together the corresponding[*] decay constants from the six cases. Although the rms difference of the six individual values from their average is often of the order of many tens of percent, the joint fits display an unexpectedly small increase in the PYWE defined in Section VI.4. In an attempt to explore this further, for both photon group structures we added an additional step in finding the joint fits. We used the average decay constants from the free fits as initial estimates for each case in turn, but allowed FPSPFT to iterate both amplitudes and decay constants away from those estimates. We then re-averaged the resulting decay constants for the final parameter set. The resulting improvement was small. In a few groups the composite fit was actually worse than before, so that we had to return to the original average.

The dashed lines in fig. 15 show the values of PYWE for the final joint fits compared to the separate (and therefore best) fits given by the solid lines. In examining this figure, we find empirically that the PYWE of the joint fit is approximately 0.6% greater than for the best fit to the 20-group electron spectrum, roughly independent of the number of terms in the fit. The corresponding differences for the 17- and 38-group photon spectra are 1.3% and 2.0%, respectively. We note also that in many cases the joint fit with m terms has both a smaller PYWE and fewer parameters than does the best fit with m-1 terms, in addition to giving a physically superior fit to the sparse data sets.

---

[*] As noted in appendix A, FPSPFT stores the decay constants in order of decreasing size. Corresponding constants are those with the same index.

# SECTION VII
## SUGGESTIONS FOR FURTHER WORK

It is clear from fig. 11 that the gradual accumulation of a more complete data base has made a very large difference in fission-product calculations since Dieckhoner's work was completed. We have also emphasized in Section III that on the average less than half of the total energy emission at times less than one minute after fission is accounted for by detailed spectra in ENDF/B-4, and in Section V.5 that fits should extend to at least $10^4$ seconds if reliable integrals to infinity are needed.

Version 5 of ENDF/B is scheduled to have more than 1,000 fission-product nuclides in its decay-property tables, including about 240 for which detailed spectral information will be included. As we pointed out in Section II, the new version will also include nuclidic yields of fission products that have been calculated using improved models for the pairing effect and the branching fraction between ground and isomeric states. Thus, it would be attractive to repeat the fitting of electron and photon spectra after Version 5 has finished its lengthy review and testing.

The computational tools for calculating the spectra are already complete. The fitting code FPSPFT can already handle extension beyond $10^3$ seconds, but needs to have an additional algorithm added that would perturb solutions after convergence in a systematic way in an extended effort to locate all of the local mimima in $\chi^2$. If experience by then has shown that AFWL's particular applications benefit from the more compact parameter set that results from using a common set of decay constants for all isotope-energy cases, it would be desirable to add rigorous simultaneous fitting of all cases to FPSPFT.

The spectrum of photons from the prompt (< 1 ns) burst has been measured for a number of cases, but the subsequent decay (1 ns to 1 ms) of isomeric states has been measured carefully only for well-moderated neutrons incident on $^{235}U$ and $^{239}Pu$. If this fragmentary information is useful, parameterization in any given group structure would be relatively straightforward.

## APPENDIX A

## MATHEMATICAL DETAILS OF FITTING DECAY CURVES

In this appendix we shall designate all vectors by unsubscripted lower-case letters, all matrices by capital letters, and all scalars by lower-case Greek letters. Our treatment basically follows that of Hamilton (ref. 19).

For each group in a given spectrum, CINDER and FPSPEC give us a table of intensities $y_i$ as a function of decay times $t_i$. For convenience, we treat these as vectors y and t, respectively. The covariances $\langle dy_i\, dy_j \rangle$ of the $y_i$ are embodied in a covariance matrix V. As mentioned in Section VI.1, we have taken V to be diagonal with elements $V_{ii} = (0.01\, y_i)^2$; that is, we have ignored correlations induced by the fact that our "data" are <u>calculated</u> from a common data base (as opposed to being independent measurements), and have arbitrarily assumed a 1% standard deviation. The weight matrix $W \equiv V^{-1}$ then causes the fit to be weighted by the <u>relative</u> error, with the generalized $\chi^2$ in units of percent$^2$.

Our task is to find m decay constants $\lambda_j$ and an equal number of amplitudes $\alpha_j$ such that the values of $\hat{y}_i$, defined by the relation

$$\hat{y}_i = \sum_{j=1}^{m} \alpha_j\, e^{-t_i \lambda_j} \ , \qquad (A1)$$

give a best fit, in the least-squares sense, to the FPSPEC values $y_i$. For convenience we shall collect the parameters $\alpha_j$ and $\lambda_j$ into a single 2m-dimensional parameter vector p such that

$$p_j = \alpha_j \qquad 0 < j \leq m$$

$$= \lambda_{j-m} \qquad m < j \leq 2m \ .$$

We put the amplitudes first in p for convenience in a preliminary linear fit using assumed initial values for the decay constants, as discussed below. All information concerning the times $t_i$ and the structure of equation A1 is then embodied in the design matrix D with elements

$$D_{ij} \equiv \frac{\partial y_i}{\partial p_j} = \qquad e^{-t_i \lambda_j} \qquad\qquad 0 < j \stackrel{\leq}{=} m \qquad\qquad \text{(A2a)}$$

$$= -t_i \, \alpha_{j-m} \, e^{-t_i \lambda_{j-m}} \qquad\qquad m < j \stackrel{\leq}{=} 2m \quad . \qquad\qquad \text{(A2b)}$$

In the usual fashion for covariant fitting, the quantity to be minimized is

$$\chi^2 \equiv d \cdot Wd = \tilde{d} \, W \, d \quad ,$$

where $d \equiv \hat{y} - y$ is the difference between the fit and the data, and $\tilde{d}$ denotes the transpose of d. We minimize $\chi^2$ by finding the value of the parameter vector p for which the gradient of $\chi^2$ with respect to p vanishes:

$$\nabla \chi^2 \quad = 2 \, \tilde{D} \, Wd = 2 \, \tilde{D} \, W \, (\hat{y}-y) = 0 \quad ,$$

and hence $\qquad\qquad \tilde{D} \, W \, \hat{y} = \tilde{D} \, W \, y \quad .$ $\qquad\qquad\qquad$ (A3)

Here we have used the chain rule to differentiate $\chi^2$ with respect to the elements $p_i$. Equation A3 is the basic form of what is traditionally called the normal equation.

Up to this point the solution is completely general and we have ignored the actual form of the design matrix in equations A2a and A2b. If the elements of the design matrix are independent of the fitted parameters, equation A3 reduces to a set of linear equations with an unique solution. Since this is not the case for equation A2, the problem is nonlinear and must be solved by iteration. We note, however, that the amplitudes $\alpha_j$ do not appear in equation A2a, so that if we assume trial values of the $\lambda_j$ we can immediately deduce the amplitudes that will minimize $\chi^2$ for that particular set of decay constants, using only the parts of p and D that correspond to $\alpha$. Thus, we can begin the solution by estimating only the decay constants $\lambda_j$.

If we designate this initial set of trial parameters by $\bar{p}$ and the corresponding initial fit by $\bar{y}$, the next step is to seek an improved parameter set p of the form

$$p = \bar{p} + q \quad , \qquad\qquad\qquad\qquad \text{(A4)}$$

in which q will be chosen to minimize $\chi^2$. This produces a corresponding change in the fit given by

46

$$\hat{y} \approx \bar{y} + D q \ , \tag{A5}$$

where we have kept only the first terms in a MacLaurin series in the small change q, and taken advantage of the fact that the first partial derivatives of $\hat{y}$ with respect to the parameters are just the elements of D. By making this approximation we have linearized the normal equation, which now reads

$$\tilde{D} W (\bar{y}+Dq) = \tilde{D} W y \ ,$$

and hence
$$(\tilde{D}WD) q = \tilde{D} W (y-\bar{y}) \ .$$

The product $N \equiv \tilde{D} W D$ is known as the normal matrix. From its inverse we can readily find a solution for q,

$$q = N^{-1} \tilde{D} W (y-\bar{y}) \ , \tag{A6}$$

in which the difference $y - \bar{y}$ is simply the error in the trial fit. Equation A6 is not rigorous because expansion A5 is not exact. However, if q is small compared to $\bar{p}$ we can expect to find that the new value of p calculated from equation A4 produces a reduction in $\chi^2$, so that by recalculating D using the new parameters we can iterate until q becomes vanishingly small.

If the first iteration <u>increases</u> $\chi^2$ we know that the initial estimate for p was too far in error for equation A5 to be a satisfactory approximation. Accordingly, in the hope that the multidimensional direction of q is more nearly correct than its length, we can replace equation A4 with

$$p = \bar{p} + q \delta \ , \tag{A7}$$

where $\delta$ is a damping constant. FPSPFT tries values of $\delta$ beginning at 1 and decreasing by a factor of 2 until a decrease in $\chi^2$ occurs or until $\delta < 10^{-5}$. If an improvement does occur, FPSPFT recalculates D and q from the successful parameters, doubles the previous value of $\delta$, and tries again. Usually it can continue doubling in each subsequent iteration until the value of $\delta$ returns to unity.

When q is large, it may produce such large changes in p that one of the decay constants will be displaced past one of its neighbors. If this happens, even if a decrease in $\chi^2$ would result, it is treated as an unsuccessful iteration, and the damping constant is reduced successively until each decay constant is at least 10% greater than the one below it (reduced to 5% after five iterations).

FPSPFT stops at a preset number of iterations (usually 25) unless the solution converges sooner. The criterion for convergence is that $\chi^2$ decrease by less than a small fraction $\epsilon$ of its previous value. After the first iteration (for which <u>any</u> decrease is acceptable), $\epsilon$ is set to $10^{-8}$. Thereafter it is doubled in each iteration, so that the definition of convergence becomes increasingly less restrictive.[*] This procedure allows FPSPFT to work with slightly overdetermined cases without wasting an inordinate amount of time trying to get $\chi^2$ ever closer to zero. It also terminates a fruitless search for a minimum that is too poorly defined to merit accurate parameters.

In Section VI.1 we discussed two methods of generating initial estimates of the decay parameters that are required to begin the iterative search. One of these is to use the solution from the previous group, and the other makes use of the empirical logarithmic slope of the decay curve. The latter method, which we attempt only for the dense data sets, requires an automatic means of defining regions in the decay curve for which the logarithmic slope $\lambda \equiv -d(\log y)/dt$ of the intensity $y$ is nearly constant for an extended interval. This means that we seek regions in which the second and third derivatives of $\log y$ are both small compared to $\log y$ itself. We have found by trial and error that the product of the normalized second and third derivatives is a simple and satisfactory measure of this property, so FPSPFT simply chooses values of $\lambda$ that correspond to minima in this product, beginning with the least positive minimum. The selected values are then sorted into descending order.

The four remaining methods that FPSPFT uses to find initial estimates produce equispaced values in a relatively blind attempt to explore the parameter space within which the decay constants are expected to lie. We begin by estimating the logarithmic slopes at the beginning and end of the time interval 0.1 to $10^3$ seconds, which we term $\lambda_b$ and $\lambda_e$, respectively. For the dense sets we take these directly from the empirical analysis. For the sparse sets we take

$$\lambda_b = \log(y_1/y_2)/(t_2 - t_1)$$

---

[*]Since $2^{25} \times 10^{-8} = 0.34$, there is clearly no reason to attempt more than 25 iterations under this definition of convergence.

and
$$\lambda_e = \log(y_{n-1}/y_n)/(t_n - t_{n-1}) \quad , \tag{A8}$$

where there are n decay-times in the data set. FPSPFT includes an option[*]
to extrapolate $\lambda_e$ approximately to $t_n$, rather than using the average of $t_{n-1}$
and $t_n$ implied by equation A8. Setting $r \equiv \lambda_e/\lambda_b$, we then define three con-
stants:

$$\delta_w \equiv r^{1/(m-1)} \qquad \text{wide}$$

$$\delta_m \equiv r^{1/m} \qquad \text{medium}$$

$$\delta_n \equiv r^{1/(m+1)} \quad , \qquad \text{narrow}$$

where m is the number of terms in the fit and the subscripts stand for the
indicated adjectives. These constants are used to generate the four geometric
series of decay constants shown in table A1. The wide equispaced set spans

## Table A1

### EQUISPACED ESTIMATES OF DECAY CONSTANTS

| Index | Spacing High | Wide | Narrow | Low |
|-------|------|------|--------|-----|
| 1 | $\lambda_b\, \delta_m$ | $\lambda_b$ | $\lambda_b\, \delta_n$ | $\lambda_b$ |
| 2 | $\lambda_b\, \delta_m^{\ 2}$ | $\lambda_b\, \delta_w$ | $\lambda_b\, \delta_n^{\ 2}$ | $\lambda_b\, \delta_m$ |
| 3 | $\lambda_b\, \delta_m^{\ 3}$ | $\lambda_b\, \delta_w^{\ 2}$ | $\lambda_b\, \delta_n^{\ 3}$ | $\lambda_b\, \delta_m^{\ 2}$ |
| . | . | . | . | . |
| . | . | . | . | . |
| . | . | . | . | . |
| m - 1 | $\lambda_e/\delta_m$ | $\lambda_e/\delta_w$ | $\lambda_e/\delta_n^{\ 2}$ | $\lambda_e/\delta_m^{\ 2}$ |
| m | $\lambda_e$ | $\lambda_e$ | $\lambda_e/\delta_n$ | $\lambda_e/\delta_m$ |

---

[*] In Section VI.3 we refer to this as the L Option.

the interval from $\lambda_b$ to $\lambda_e$ in equal logarithmic steps. The narrow equispaced set is compressed so that it is wholly interior to the same interval. The high and low equispaced sets use an intermediate spacing, and are offset so as to end on $\lambda_e$ or begin on $\lambda_b$, respectively. FPSPFT does not use estimates that lie outside the empirical range, since we have found that it is easy for the iteration process to move parameters outwards from within the range but sometimes is difficult to move inwards from outside the range.

## APPENDIX B

## FORMAT OF TRANSMITTAL CARDS

We have used two different formats for the punched cards that contain
the parameter sets that describe the fitted decay curves. The first form is
used for the free fits (or best fits), which have different decay constants
for each energy-isotope case. The data are organized into self-contained
decks, of which an example is shown in fig. B1 for the 6-term fit to the 17-
group photon spectrum from case 49H. Most of the format is explained by an-
notations in the figure. The information at the end of the deck-heading card
correlates the cards with their corresponding printed output. The primary
information is a succession of $\underline{pairs}$ of parameters $(\lambda_i, \alpha_i)$ for the successive
terms in equation A1. A separate subtable in this form is given for each
group.

The second form of transmittal cards is used for the joint fits, in which
a single set of decay constants serves all six energy-isotope cases. Since
this parameter set emphasizes compactness, we have used a card format that
minimizes wasted space on the cards. Figure B2 shows the beginning and end
of the 17-group photon parameter set, together with an intermediate portion
of the set. In this format we have used descriptive heading cards to make the
format as nearly self-explanatory as possible. Here the boundaries of the
group structure, which is constant for the entire set, are given first. Next
we give the decay constants for all 2-term fits, followed by separate sub-
tables of the amplitudes for each 2-term fit, and so on for each number of
terms in succession. Consequently, the primary information consists of a
list of values (not pairs of values) of a particular type of parameter for
successive groups in the spectrum.

In both forms all of the significant integer information is given in
fields with Fortran format I5 that end on a multiple of 5 columns. The energy
widths and boundaries of the group structure are in F5.2 format in fields that
also end on multiples of 5 columns. All other floating-point values are in
E10.3 fields that end on a multiple of 10 columns.

Atomic number of fissioning nucleus
— Mass  "  "  "  "
————— Neutron energy ( 1 = thermal, 2 = fission, 3 = 14 MeV )
————— Type of particle ( 1 = electron, 2 = photon )
————— Number of groups in spectrum
————— Number of terms fitted
————— Date and time cards were punched

```
94   239      3    2   17    6   8/12/77   4.01.41      LAMBDA          1
   1  6.25    .75 ◄————————— Group 1 upper energy and width (MeV)
3.308E+00 1.049E-04 1.311E+00 5.076E-05 1.813E-01 8.989E-05 6.483E-02 3.159E-06
1.922E-02 3.714E-06 1.266E-02 3.177E-06      ◄— λ₃      ◄— a₃      ◄— λ₄      ◄— a₄
   2  5.50    .50
3.229E+00 9.755E-05 1.233E+00 4.293E-05 1.788E-01 7.801E-05 3.011E-02 2.691E-06
1.145E-02 6.366E-06 4.034E-03 1.814E-06
   3  5.00    .50 ◄————————— Group 3 upper energy and width
3.210E+00 7.113E-05 1.266E+00 3.286E-05 1.770E-01 6.014E-05 1.097E-02-3.587E-06
9.901E-03 7.278E-06 3.899E-03 2.146E-06
   4  4.50    .50
2.812E+00 2.124E-04 7.886E-01 5.620E-05 4.782E-02 5.756E-05 1.471E-02 6.966E-05
7.782E-03 2.465E-05 3.598E-03 1.292E-05
   5  4.00    .50
3.082E+00 2.895E-04 1.098E+00 1.230E-04 3.929E-02 1.149E-04 1.375E-02 1.263E-04
5.244E-03 1.720E-05 1.130E-03 3.486E-06
   6  3.50    .50
2.938E+00 2.392E-04 9.533E-01 7.623E-05 6.398E-02 7.312E-05 1.749E-02 6.997E-05
6.386E-03 4.597E-05 1.581E-03 9.698E-06
   7  3.00    .50
2.389E+00 1.284E-03 3.186E-01-1.763E-04 6.410E-02 7.368E-04 1.890E-02 3.323E-04
8.086E-03 1.152E-04 9.699E-04 1.382E-05
   8  2.50    .50
3.207E+00 9.103E-04 1.225E+00 4.552E-04 9.551E-02 3.375E-04 2.791E-02 3.487E-04
9.686E-03 2.127E-04 7.210E-04 2.924E-05
   9  2.00    .50
2.925E+00 3.559E-03 8.993E-01 1.074E-03 1.052E-01 1.408E-03 2.731E-02 1.043E-03
9.320E-03 3.190E-04 8.787E-04 5.263E-05
  10  1.50    .50
2.815E+00 1.621E-02 7.867E-01 4.349E-03 1.146E-01 6.835E-03 2.889E-02 2.831E-03
9.434E-03 1.575E-03 8.897E-04 1.674E-04
  11  1.00    .25
2.259E+00 6.847E-02 6.579E-01 7.151E-02 1.212E-01 4.643E-03 2.842E-02 1.541E-03
7.097E-03 5.521E-04 7.962E-04 1.969E-04
  12   .75    .25
2.671E+00 9.824E-02 3.668E-01 6.616E-02 1.057E-01 2.046E-02 2.532E-02 2.778E-03
7.764E-03 7.557E-04 9.149E-04 1.848E-04
  13   .50    .25
2.665E+00 6.787E-02 3.491E-01 2.957E-02 1.098E-01 2.987E-02 2.619E-02 3.063E-05
6.579E-03 1.038E-03 8.686E-04 3.398E-04
  14   .25    .10
2.859E+00 4.764E-03 8.052E-01 1.311E-03 1.026E-01 1.808E-03 2.633E-02 1.360E-03
6.798E-03 3.185E-04 1.269E-03 1.461E-04
  15   .15    .05
2.176E+00 6.363E-02 6.582E-01 6.897E-02 9.470E-02 2.842E-03 2.843E-02 6.224E-04
7.158E-03 7.986E-05 7.092E-04 2.060E-05
  16   .10    .05
2.365E+00 7.209E-04 2.751E-01-2.038E-04 5.615E-02 4.035E-04 1.488E-02 2.414E-04
5.269E-03 1.126E-04 9.183E-04 3.191E-055 ◄—— Group 17 upper energy and width
  17   .05    .05
3.143E+00 3.412E-04 1.089E+00 1.023E-04 1.066E-01-2.522E-04 3.451E-02 2.715E-04
6.562E-03 1.894E-04 9.756E-04 1.884E-04      ◄— λ₃   ◄— a₃   ◄— λ₄   ◄— a₄
   ◄— λ₅      ◄— a₅      ◄— λ₆      ◄— a₆
```

Figure B1.  Transmittal Card Format for Free Fits (Annotated)

52

Top of group 1

17-GROUP ENERGY BOUNDARIES
6.25 5.50 5.00 4.50 4.00 3.50 3.00 2.50 2.00 1.50 1.00 .75 .50 .25 .15 .10
.05 0.00 ◄——————————— Bottom of group 17          ————— Applies to all 6 cases    Group
    2-TERM DECAY CONSTANTS FOR EACH GROUP ◄————                17 GROUPS                    7
    1          1.944E-01 1.852E-01 1.927E-01 2.314E-02 2.003E-02 5.721E-02 3.026E-02   1st
3.065E-02 3.424E-02 4.963E-02 5.615E-01 1.936E-01 1.589E-01 4.078E-02 5.435E-01    term
2.419E-02 2.248E-02 ◄————————— Decay constant for 1st term in group 17
    2          1.324E-02 5.417E-03 4.951E-03 4.494E-03 2.461E-03 3.786E-03 1.965E-03   2nd
1.530E-03 1.716E-03 2.192E-03 3.852E-03 3.655E-03 2.634E-03 1.798E-03 4.329E-03    term
2.061E-03 1.381E-03
    AMPLITUDES FOR    92 235  GAMMA    FAST        17 GROUPS        2 TERMS
    1          4.687E-04 4.008E-04 3.133E-04 3.211E-04 5.708E-04 3.644E-04 2.448E-03   1st
2.024E-03 4.984E-03 2.369E-02 2.628E-01 1.524E-01 8.445E-02 8.425E-03 2.869E-01    term
1.428E-03 5.995E-05 ◄————————— Amplitude of 1st term in group 17 for case 25F
    2          9.968E-06 1.380E-05 1.287E-05 7.305E-05 2.395E-05 9.177E-05 5.335E-05   2nd
9.323E-05 1.416E-04 6.379E-04 1.124E-03 1.377E-03 1.302E-03 2.457E-04 2.056E-04    term
9.852E-05 1.465E-04 ◄————————— Amplitude of 2nd term in group 17 for case 25F
    ————— Group 16

                                                     .
                                                     .
                                                     .
    3-TERM DECAY CONSTANTS FOR EACH GROUP                17 GROUPS
    1          2.936E+00 2.068E-01 4.728E-01 2.330E+00 2.377E+00 1.628E+00 1.881E-01   1st
1.401E+00 1.442E+00 5.189E-01 7.199E-01 2.306E-01 2.276E-01 1.580E+00 6.711E-01    term
2.991E+00 3.145E+00
    2          1.581E-01 1.499E-02 5.294E-02 1.835E-02 1.743E-02 1.789E-02 1.960E-02   2nd
2.208E-02 2.625E-02 2.516E-02 3.301E-02 2.144E-02 2.376E-02 3.123E-02 4.137E-02    term
2.095E-02 6.974E-03
    3          1.324E-02 4.342E-03 4.503E-03 4.307E-03 2.336E-03 2.627E-03 1.600E-03   3rd
1.289E-03 1.473E-03 1.459E-03 1.644E-03 1.505E-03 1.287E-03 1.520E-03 1.469E-03    term
1.948E-03 4.985E-04
    AMPLITUDES FOR    92 235  GAMMA    FAST        17 GROUPS        3 TERMS
    1          5.587E-04 4.181E-04 3.915E-04 5.347E-04 8.003E-04 7.213E-04 2.028E-03   1st
3.851E-03 6.518E-03 3.418E-02 3.017E-01 1.377E-01 9.080E-02 1.187E-02 3.146E-01    term
1.618E-03 1.381E-04
    2          3.500E-04 1.294E-05 3.877E-05 2.618E-04 4.778E-04 2.031E-04 1.298E-03   2nd
1.499E-03 3.660E-03 1.144E-02 5.318E-03 5.672E-03 4.873E-03 6.134E-03 5.528E-03    term
1.234E-03 1.229E-04
    3          9.813E-06 6.915E-06 9.668E-06 6.351E-05 2.171E-05 3.779E-05 4.080E-05   3rd
7.293E-05 1.164E-04 3.866E-04 4.850E-04 3.585E-04 5.364E-04 1.975E-04 3.871E-05    term
8.977E-05 7.466E-05

                                                     .
                                                     .
                                                     .

    AMPLITUDES FOR    94 239  GAMMA    14-MEV      17 GROUPS        6 TERMS
    1          1.459E-04 1.311E-04 7.958E-05 2.229E-04 3.603E-04 2.351E-04 1.331E-03   1st
8.953E-04 2.875E-03 1.661E-02 6.617E-02 1.193E-01 7.283E-02 5.457E-03 6.587E-02    term
7.240E-04 4.494E-04
    2          2.247E-05 1.991E-05 3.885E-05 6.015E-05 7.268E-05 8.611E-05 -1.312E-04  2nd
5.260E-04 1.926E-03 4.867E-03 6.931E-02 7.131E-02 3.506E-02 1.294E-03 6.449E-02    term
-1.346E-04 1.180E-04
    3          8.616E-05 7.353E-05 5.785E-05 5.026E-05 3.694E-05 6.340E-05 6.807E-04   3rd
3.861E-04 1.383E-03 6.337E-03 4.577E-03 1.657E-02 2.642E-02 1.697E-03 1.900E-03    term
3.604E-04 -2.744E-04
    4          2.663E-06 4.364E-06 1.574E-07 4.875E-05 1.712E-04 8.500E-05 3.740E-04   4th
2.912E-04 1.084E-03 2.967E-03 1.519E-03 2.726E-03 2.744E-03 9.663E-04 6.803E-04    term
2.443E-04 2.630E-04
    5          5.092E-06 4.884E-06 3.453E-06 4.189E-05 4.590E-05 5.265E-05 1.184E-04   5th
1.421E-04 2.956E-04 1.458E-03 5.282E-04 6.337E-04 1.031E-03 3.727E-04 7.950E-05    term
1.045E-04 2.049E-04
    6          3.137E-06 1.928E-06 2.359E-06 1.429E-05 4.819E-06 9.885E-06 1.308E-05   6th
2.833E-05 5.235E-05 1.625E-04 1.931E-04 1.868E-04 3.289E-04 1.171E-04 2.324E-05    term
3.344E-05 1.369E-04

Figure B2.  Transmittal Card Format for Joint Fits (Annotated)

53

APPENDIX C

FORMAT OF PRINTED OUTPUT FROM FPSPFT

The printout from the fitting program FPSPFT is organized into five tables, with some information displayed in more than one table. Samples of these tables for a 9-group beta spectrum (chosen to limit the fifth table to a single page) are shown in figs. C1 through C5. Again, these figures are liberally annotated and should be nearly self-explanatory. All except the fourth table use the same three lines for a page heading.

The original purpose of the first output table was to summarize the struggle to find the absolute minimum in $\chi^2$, and that is what we illustrated in fig. C1. In practice, however, the listings delivered to AFWL are the product of the additional analysis described in Sections VI.3 and VI.6, and hence are made by dictating fixed decay constants and refitting only the amplitudes. Accordingly, they include further information between lines 3 and 4 of fig. C1 to identify the imposed set of decay constants, and the table contains only the first of the six columns.

The second output table, as shown in fig. C2, displays the fitted parameters. For the free fits, the transmittal cards are essentially equivalent to reading this table across the rows in turn. For the joint fits, the columns headed lambda are punched first (they are, of course, the same for each energy-isotope case). Then the amplitudes are punched, again reading down the columns.

The third table contains the most detailed information regarding the fits, and hence is too crowded to explain each column directly in fig. C3. The meanings of the column headings are fairly evident, but require some additional explanation:

GROUP      Number of the group.

MEV        Upper energy of the group.

ITER       Total number of iterations to reach convergence. In the final listings this appears as 0 because the decay constants were dictated.

DAMP      Smallest value of the damping constant (see equation A7) required to achieve the fit to this group. Here, again, the final listings always give 1.0 since no iteration was required. Below the value of DAMP for each group, this column is used to number the times in the SECONDS column.

SECONDS   Decay time since the end of the fission pulse.

54
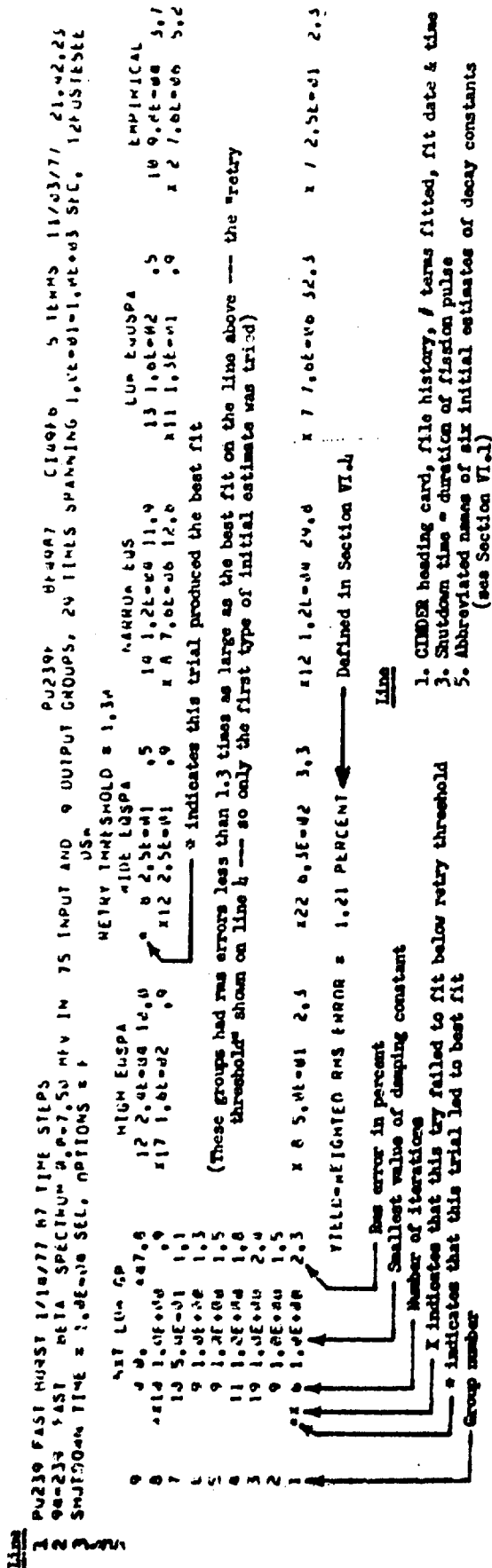
Figure C1. Example of First Output Table (Annotated). This table summarizes the fits achieved from different initial estimates of decay constants.
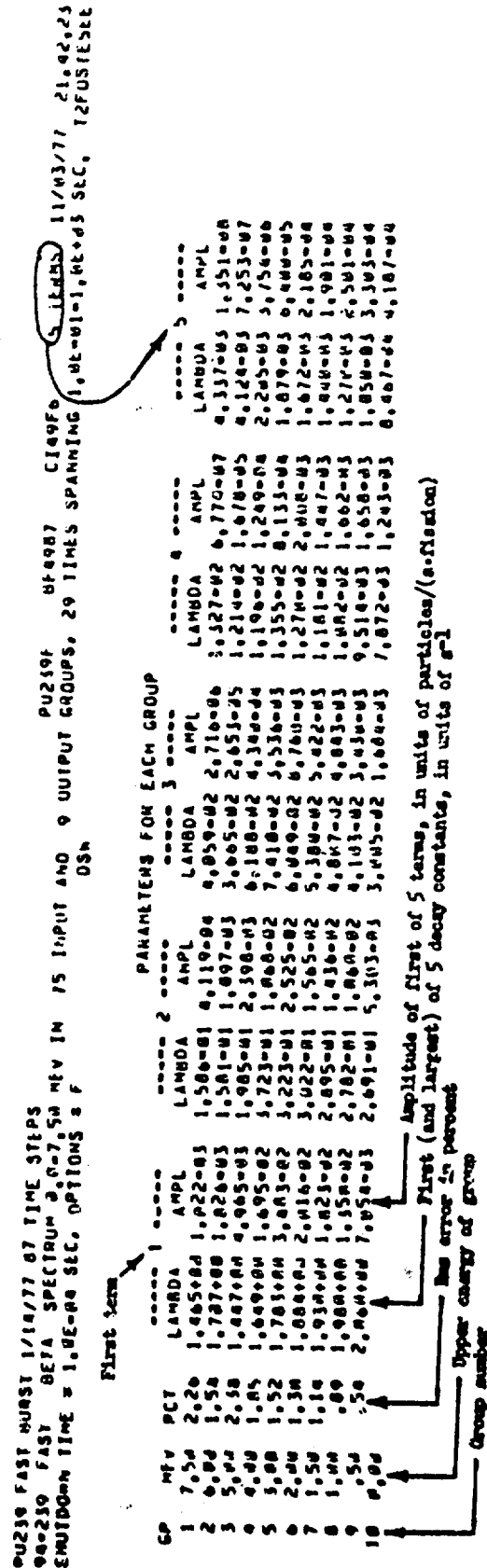
Figure C2. Example of Second Output Table (Annotated). These are the adopted fitted parameters.

55

Source of initial decay constants that yielded best fit

Fit error exceeded 1.3 times error in group 2

FIT FAILED

Fraction of integral to infinity

Integral from 0 to 1000 s, in particles/(MeV·fission)

(This fit is better than the retry threshold calculated from group 3)

Markers of trial and final decay constants

**Figure C3.** Example of Beginning of Third Output Table (Annotated). The column headings are defined in this appendix.

DATA      Intensities in this group calculated by CINDER/FPSPEC. These are in particles/(MeV·s·fission), not in particles/(s·fission).

PCT.DIF.   FIT-DATA expressed in percent of DATA. The rms value of PCT.DIF. for this group appears below the last time-step.

FIT       Intensities calculated from the fitted parameters, in the same units as DATA.

TAU       Empirical mean life (reciprocal of the decay constant) in seconds, determined by fitting a Lagrange polynomial to the logarithm of the data, as described in Section VI.1. For sparse data sets the apparent mean life implied by pairs of adjacent times is used instead.*

CURV      Normalized first derivative of TAU.

DEP       Product of CURV and the normalized 2nd derivative of TAU.

LAMBDA    Fitted decay constants, in units of $s^{-1}$.

AMPLITUDE Fitted amplitudes, in particles/(s·fission).

FRACT.    Fraction of the integrated yield from 0 to infinite time that comes from this term.

    Between the columns labelled FIT and TAU appear asterisks and numerals. These are intended to be read as graphical marks against the time scale implied by TAU. The numerals mark the assumed mean lives with which the fit began, and the asterisks show how far these migrated during iteration. Both are rounded to the nearest row in the TAU scale.

    The fourth output table (fig. C4) shows the comparison between the sum of DATA over all groups and the sum of FIT over all groups. The three types of rms error are discussed in Section VI.4.

    The final table is illustrated in fig. C5. All of the information in this table is reconstructed from the fitted parameters. In principal, almost all of it occurs in the third table also, but here we have converted the units to group constants by multiplying each fitted intensity by the width of its group. We have also extrapolated the table backwards to zero time and forwards to $10^5$ seconds. We have discussed the accuracy of this extrapolation in Section VI.5. The total number of particles per fission integrated to infinite time appears only in this fifth table.

----

*A rule of thumb that was widely used in the very early days of Civil Defense states that the current decay constant is equal to the reciprocal of the time since fission. This approximation implies a $t^{-1}$ decay curve. The difference between SECONDS and TAU is a measure of the inaccuracy of the $t^{-1}$ approximation.

## TOTAL YIELD VS. TIME

ACTUAL S.D. = 1.02 PCT    PREDICTED S.D. = 1.60 PCT →

Rms of "pct.dif." column (left annotation, arrow pointing to ACTUAL S.D.)

Rms error of all groups and times (right annotation, arrow pointing to PREDICTED S.D.)

| | SECONDS | DATA | PCT.DIF. | FIT |
|---|---|---|---|---|
| 1 | 1.0E-01 | 2.224E-01 | -.92 | 2.204E-01 |
| 2 | 1.5E-01 | 2.112E-01 | -.37 | 2.104E-01 |
| 3 | 2.0E-01 | 2.012E-01 | .06 | 2.013E-01 |
| 4 | 4.0E-01 | 1.697E-01 | .84 | 1.711E-01 |
| 5 | 5.0E-01 | 1.579E-01 | .83 | 1.592E-01 |
| 6 | 6.0E-01 | 1.479E-01 | .67 | 1.489E-01 |
| 7 | 8.0E-01 | 1.321E-01 | .12 | 1.323E-01 |
| 8 | 1.0E+00 | 1.202E-01 | -.47 | 1.196E-01 |
| 9 | 1.5E+00 | 9.979E-02 | -1.27 | 9.852E-02 |
| 10 | 2.0E+00 | 8.640E-02 | -1.02 | 8.552E-02 |
| 11 | 4.0E+00 | 5.779E-02 | 1.27 | 5.852E-02 |
| 12 | 5.0E+00 | 4.996E-02 | 1.18 | 5.055E-02 |
| 13 | 6.0E+00 | 4.418E-02 | .58 | 4.444E-02 |
| 14 | 8.0E+00 | 3.619E-02 | -.84 | 3.588E-02 |
| 15 | 1.0E+01 | 3.087E-02 | -1.59 | 3.038E-02 |
| 16 | 1.5E+01 | 2.291E-02 | -.66 | 2.276E-02 |
| 17 | 2.0E+01 | 1.841E-02 | 1.24 | 1.864E-02 |
| 18 | 4.0E+01 | 1.057E-02 | 1.38 | 1.071E-02 |
| 19 | 5.0E+01 | 8.746E-03 | -.04 | 8.742E-03 |
| 20 | 6.0E+01 | 7.448E-03 | -.96 | 7.376E-03 |
| 21 | 8.0E+01 | 5.704E-03 | -1.19 | 5.637E-03 |
| 22 | 1.0E+02 | 4.582E-03 | -.31 | 4.568E-03 |
| 23 | 1.5E+02 | 3.008E-03 | 1.31 | 3.047E-03 |
| 24 | 2.0E+02 | 2.211E-03 | .59 | 2.224E-03 |
| 25 | 4.0E+02 | 1.080E-03 | -1.94 | 1.059E-03 |
| 26 | 5.0E+02 | 8.737E-04 | -.39 | 8.704E-04 |
| 27 | 6.0E+02 | 7.399E-04 | 1.12 | 7.482E-04 |
| 28 | 8.0E+02 | 5.725E-04 | 1.61 | 5.818E-04 |
| 29 | 1.0E+03 | 4.682E-04 | -1.26 | 4.623E-04 |

YIELD-WEIGHTED RMS ERROR = 1.21 PERCENT
(defined in Section VI.4)

Figure C4. Example of Fourth Output Table (Annotated). This table compares the sum of the fitted spectrum to the sum given by CINDER.

Figure C5. Example of Fifth Output Table. This table is reconstructed from the fitted parameters.

# REFERENCES

1.  Stovall, R. L., _Time Dependence of the Beta Spectrum from the Fission Products of a Thermonuclear Weapon_, GSP/Phys/64-13, thesis submitted to the Air Force Institute of Technology, Wright-Patterson Air Force Base, OH, November 1964.

2.  Dieckhoner, J. E., _Prediction of the Time-Dependent Beta Spectrum from a Nuclear Weapon Detonation_, GNE/Phys/65-3 (AD 621 023), Air Force Institute of Technology, Wright-Patterson Air Force Base, OH, August 1965.

3.  England, T. R., and Schenter, R. E., _ENDF/B-IV Fission-Product Files: Summary of Major Nuclide Data_, LA-6116-MS (ENDF-223), Los Alamos Scientific Laboratory, October 1975.

4.  Madland, D. G., and England, T. R., _The Influence of Pairing on the Distribution of Independent Yield Strengths in Neutron-Induced Fission_, LA-6430-MS (ENDF-240), Los Alamos Scientific Laboratory, July 1976.

5.  Madland, D. G., and England, T. R., _Distribution of Independent Fission-Product Yields to Isomeric States_, LA-6595-MS (ENDF-241), Los Alamos Scientific Laboratory, November 1976.

6.  England, T. R., _CINDER -- A One-Point Depletion and Fission-Product Program_, WAPD-TM-334 (Rev), 1964; England, T. R., Wilczynski, B., and Whittemore, N. L., _CINDER-7: An Interim Report for Users_, LA-5885-MS, Los Alamos Scientific Laboratory, April 1975.

7.  Stamatelatos, M. G., and England, T. R., _FPDCYS and FPSPEC, Computer Programs for Calculating Fission-Product Beta and Gamma Multigroup Spectra from ENDF/B-IV Data_, LA-NUREG-6818-MS, Los Alamos Scientific Laboratory, May 1977.

8.  England, T. R., and Stamatelatos, M. G., _Multigroup Beta and Gamma Spectra of Individual ENDF/B-IV Fission-Product Nuclides_, LA-NUREG-6622-MS, Los Alamos Scientific Laboratory, December 1976.

9.  Schenter, R. E., Ed., _Benchmark Test of ENDF/B-IV_, (ENDF-230), Fission Product Section, Vol. 1, Brookhaven National Laboratory, 1976.

10. England, T. R., and Stamatelatos, M. G., _Comparisons of Calculated and Experimental Delayed Fission-Product Beta and Gamma Spectra from $^{235}$U Thermal Fission_, LA-NUREG-6896-MS, Los Alamos Scientific Laboratory, July 1977.

11. Schmittroth, F., and Schenter, R. E., "Uncertainties in Fission-Product Decay-Heat Calculations," _Nucl. Sci. Eng. 63_, pp. 276-291, 1977.

12. England, T. R., Stamatelatos, M. G., Schenter, R. E., and Schmittroth, F., _Fission-Product Source Terms for Reactor Applications_, LA-NUREG-6917-MS, Los Alamos Scientific Laboratory, August 1977.

13. Schmittroth, F., and Schenter, R. E., "Application of Least-Squares Method to Decay-Heat Evaluation," submitted for publication in Nucl. Sci. Eng., 1977.

14. Tsoulfanidis, N., Wehring, B. W., and Wyman, M. E., "Measurements of Time-Dependent Energy Spectra of Beta Rays from Uranium-235 Fission Products," Nucl. Sci. Eng. 43, pp. 42-53, 1971.

15. Dickens, J. K., et al., Fission-Product Energy Release of $^{235}U$ between 2 and 14 000 Sec, ORNL/NUREG-14 (draft), Oak Ridge National Laboratory, April 1977.

16. LaBauve, R. J., England, T. R., Stamatelatos, M. G., and George, D. C., Approximations to Summation Calculations of Delayed Energy and Spectra, LA-6684-MS, Los Alamos Scientific Laboratory, January 1977.

17. England, T. R., Stamatelatos, M. G., and LaBauve, R. J., Burst Functions, Tabular Data, and Plots for Use in Generating the ANS 5.1 Decay-Heat Standard, LA-UR-77-627, Los Alamos Scientific Laboratory, March 1977.

18. Foster, D. G. Jr., and England, T. R., "Time-Dependent Spectra of Photons and Spontaneous-Fission Neutrons for Applied Problems, "Trans. Am. Nucl. Soc. 23, p. 551, 1976.

19. Hamilton, W. C., Statistics in Physical Science, chap. 4, Ronald Press, New York, 1964.